JOURNAL OF PETROLOGY | VOLUME 0 | NUMBER 0 | PAGES 1–34 | 2010 | doi:10.1093/petrology/egq062
Journal of Petrology Advance Access published November 18, 2010

The Role of Water in Generating the Calc-alkaline Trend: New Volatile Data for Aleutian Magmas and a New Tholeiitic Index

MINDY M. ZIMMER[1]*, TERRY PLANK[1]†, ERIK H. HAURI[2], GENE M. YOGODZINSKI[3], PETER STELLING[4], JESSICA LARSEN[5], BRAD SINGER[6], BRIAN JICHA[6], CHARLES MANDEVILLE[7] AND CHRISTOPHER J. NYE[8]

[1]DEPARTMENT OF EARTH SCIENCES, BOSTON UNIVERSITY, BOSTON, MA 02215, USA

[2]DEPARTMENT OF TERRESTRIAL MAGNETISM, CARNEGIE INSTITUTION OF WASHINGTON, WASHINGTON, DC 20015, USA

[3]DEPARTMENT OF GEOLOGICAL SCIENCES, UNIVERSITY OF SOUTH CAROLINA, COLUMBIA, SC 29208, USA

[4]GEOLOGY DEPARTMENT, WESTERN WASHINGTON UNIVERSITY, BELLINGHAM, WA 98225, USA

[5]ALASKA VOLCANO OBSERVATORY, GEOPHYSICAL INSTITUTE, UNIVERSITY OF ALASKA FAIRBANKS, FAIRBANKS, AK 99775, USA

[6]GEOLOGY AND GEOPHYSICS, UNIVERSITY OF WISCONSIN, MADISON, WI 53706, USA

[7]DEPARTMENT OF EARTH AND PLANETARY SCIENCES, AMERICAN MUSEUM OF NATURAL HISTORY, NEW YORK, NY 10024, USA

[8]ALASKA VOLCANO OBSERVATORY, ALASKA DIVISION OF GEOLOGICAL AND GEOPHYSICAL SURVEYS, FAIRBANKS, AK 99775, USA

RECEIVED DECEMBER 9, 2010; ACCEPTED SEPTEMBER 16, 2010

The origin of tholeiitic (TH) versus calc-alkaline (CA) magmatic trends has long been debated. Part of the problem stems from the lack of a quantitative measure for the way in which a magma evolves. Recognizing that the salient feature in many TH–CA discrimination diagrams is enrichment in Fe during magma evolution, we have developed a quantitative index of Fe enrichment, the Tholeiitic Index (THI): THI = $Fe_{4\cdot0}/Fe_{8\cdot0}$, where $Fe_{4\cdot0}$ is the average FeO concentration of samples with 4 ± 1 wt % MgO, and $Fe_{8\cdot0}$ is the average FeO* at 8 ± 1 wt % MgO. Magmas with THI > 1 have enriched in FeO* during differentiation from basalts to andesites and are tholeiitic; magmas with THI < 1 are calc-alkaline. Most subduction zone volcanism is CA, but to varying extents; the THI expresses the continuum of Fe enrichment observed in magmatic suites in all tectonic settings. To test various controls on the development of CA trends, we present new magmatic water measurements in melt inclusions from eight volcanoes from the Aleutian volcanic arc (Augustine, Emmons, Shishaldin, Akutan, Unalaska, Okmok, Seguam, and Korovin). Least degassed H_2O contents vary from ~2 wt % (Shishaldin) to >7 wt % (Augustine), spanning the global range in arc mafic magmas. Within the Aleutian data, H_2O correlates negatively with THI, from strongly calc-alkaline (Augustine, THI = 0·65) to moderately tholeiitic (Shishaldin, THI = 1·16). The relationship between THI and magmatic water is maintained when data are included from additional arc volcanoes, back-arc basins, ocean islands, and mid-ocean ridge basalts (MORBs), supporting a dominant role of magmatic water in generating CA trends. An effective break between TH and CA trends occurs at ~2 wt % H_2O. Both pMELTs calculations and laboratory experiments demonstrate that the observed co-variation of H_2O and THI in arcs can be generated by the effect of H_2O on the*

*Corresponding author. Present address: ExxonMobil Research and Engineering Co., Annandale, NJ 08809, USA. Telephone: (908) 442-6602. Fax: (908) 730-3314. E-mail: mindy.zimmer@gmail.com

†Present address: Lamont–Doherty Earth Observatory and Department of Earth and Environmental Sciences, Columbia University, Palisades, NY 10964, USA.

suppression of plagioclase and the relative enhancement of Fe-oxides on the liquid line of descent. The full THI–H_2O array requires an increase in fO_2 with H_2O, from ≤FMQ (where FMQ is the fayalite–magnetite–quartz buffer) in MORB to ~ΔFMQ +0·5 to +2 in arcs, consistent with inferences from measured Fe and S species in glasses and melt inclusions. A curve fit to the data, H_2O (wt % ± 1·2) = exp[(1·26 − THI)/0·32], may provide a useful tool for estimating the H_2O content of magmas that are inaccessible to melt inclusion study.

KEY WORDS: *subduction; water; calc-alkaline; tholeiitic; Aleutian*

INTRODUCTION

The origin and evolution of magmas remains a central question in igneous petrology. One of the earliest debates was spawned by Bowen's classic theory (Bowen, 1928; Young, 1998), which emphasized silica enrichment as the dominant form of magma evolution. Fenner (1931) and others countered with examples of magmas that experience iron enrichment, most notably the Skaergaard intrusion (Wager & Deer, 1939). Now it is recognized that iron enrichment during magmatic evolution is ubiquitous in every tectonic setting on Earth. Indeed, every mid-ocean ridge magma enriches in iron as it evolves, and such a trend is reproduced well by low-pressure fractional crystallization of dry magma (Walker *et al.*, 1979; Juster *et al.*, 1989; Langmuir *et al.*, 1992). Extremely iron-enriched, end-stage liquids resulting from fractional crystallization have been observed in layered mafic intrusions from different tectonic settings (Wager & Deer, 1939; Sparks, 1988; Wiebe, 1997). In contrast, subduction zones produce magmas with a range of evolutionary trends, including pronounced iron depletion (e.g. Fenner, 1926; Chesner & Rose, 1984; Kay & Kay, 1985; Carr *et al.*, 2003; Grove *et al.*, 2003). Iron depletion is also observed in continental rift magmas (Trua *et al.*, 1999; Wang *et al.*, 2002; Krienitz *et al.*, 2007) and ocean island basalts (e.g. Muñoz García, 1969; Ibarrola Muñoz, 1970; Thirlwall *et al.*, 2000).

The enrichment vs depletion of iron in magmatic suites is generally described as tholeiitic (TH) vs calc-alkaline (CA) differentiation, respectively. Use of these terms, however, is varied and vague, with different meanings to different workers (Arculus, 2003). Certainly, the term 'calc-alkaline' has become something of a colloquialism for 'arc magma evolution'. The use of multiple discrimination diagrams (AFM, or Alkali–FeO*–MgO, and FeO*/MgO vs SiO_2, where FeO* denotes all Fe calculated as FeO; Kuno, 1968; Irvine & Baragar, 1971; Miyashiro, 1974) contributes to the ambiguity. In addition, magmas display a continuum of Fe enrichment, so assigning a magma to one of two groups is a recognized simplification.

Here we develop a quantitative index based on Fe enrichment, the Tholeiitic Index (THI), which describes the range of Fe enrichment observed in natural systems. We redefine tholeiitic (TH) and calc-alkaline (CA) magma series based on the THI and use this index to test models for the origin of CA fractionation. As an example, we use the volcanoes of the Aleutian arc, which span the global range of subduction-related TH and CA evolution and have long served as type examples for different evolutionary models (Fenner, 1926; Bowen, 1928; Kay *et al.*, 1982; Kay & Kay, 1985, 1994; Myers *et al.*, 1985; Baker & Eggler, 1987; Gust & Perfit, 1987; Brophy, 1990; Miller *et al.*, 1992; Brophy *et al.*, 1999; Kelemen *et al.*, 2003; George *et al.*, 2004). To test the relationship between magmatic water content and THI, we present the first extensive study of the water contents in Aleutian magmas, focusing on melt inclusions in mafic tephra from eight Aleutian volcanoes. We introduce Shishaldin and Augustine as end member TH and CA volcanoes, and then examine how variations in magmatic water content, pressure of crystallization, oxygen fugacity, and parental magma composition may lead to TH vs CA evolution. A strong anti-correlation between measured magmatic water concentrations and THI implicates a dominant role of water in CA fractionation, and may provide a predictive tool for estimating the water content of magmatic suites worldwide.

BACKGROUND

Terminology: tholeiitic vs calc-alkaline trends

The term 'calc-alkaline' has a long and complex history (see Arculus, 2003, for a comprehensive review of the etymology). A brief summary is given here. Two volcanic rock series were defined by Harker (1909): the Pacific Branch (richer in CaO and MgO) and the Atlantic Branch (richer in alkalis). Holmes (1918) noted that the trends SiO_2–CaO and SiO_2–alkalis ($Na_2O + K_2O$) cross at ~62 wt % SiO_2 for 'calc-alkali', Pacific Branch-type rocks. Peacock (1931) subsequently defined four subsets of magma using the SiO_2 value at which CaO and alkali trends intersected, including a 'calc-alkalic' group (intersection at 56–61 wt % SiO_2). The term 'calc-alkaline' stems from this characterization, but has evolved substantially away from it. In addition, the term 'tholeiitic' is not to be confused with 'tholeiite', referring to the olivine- and hypersthene-normative rock defined on the basalt tetrahedron. The definition of TH and CA has evolved with the popular AFM diagram (Irvine & Baragar, 1971) and FeO*/MgO–SiO_2 diagram (Miyashiro, 1974), which emphasize Fe enrichment (TH) or depletion (CA; Gill, 1981; Arculus, 2003). Here we also consider Fe enrichment the fundamental feature of a TH magmatic suite.

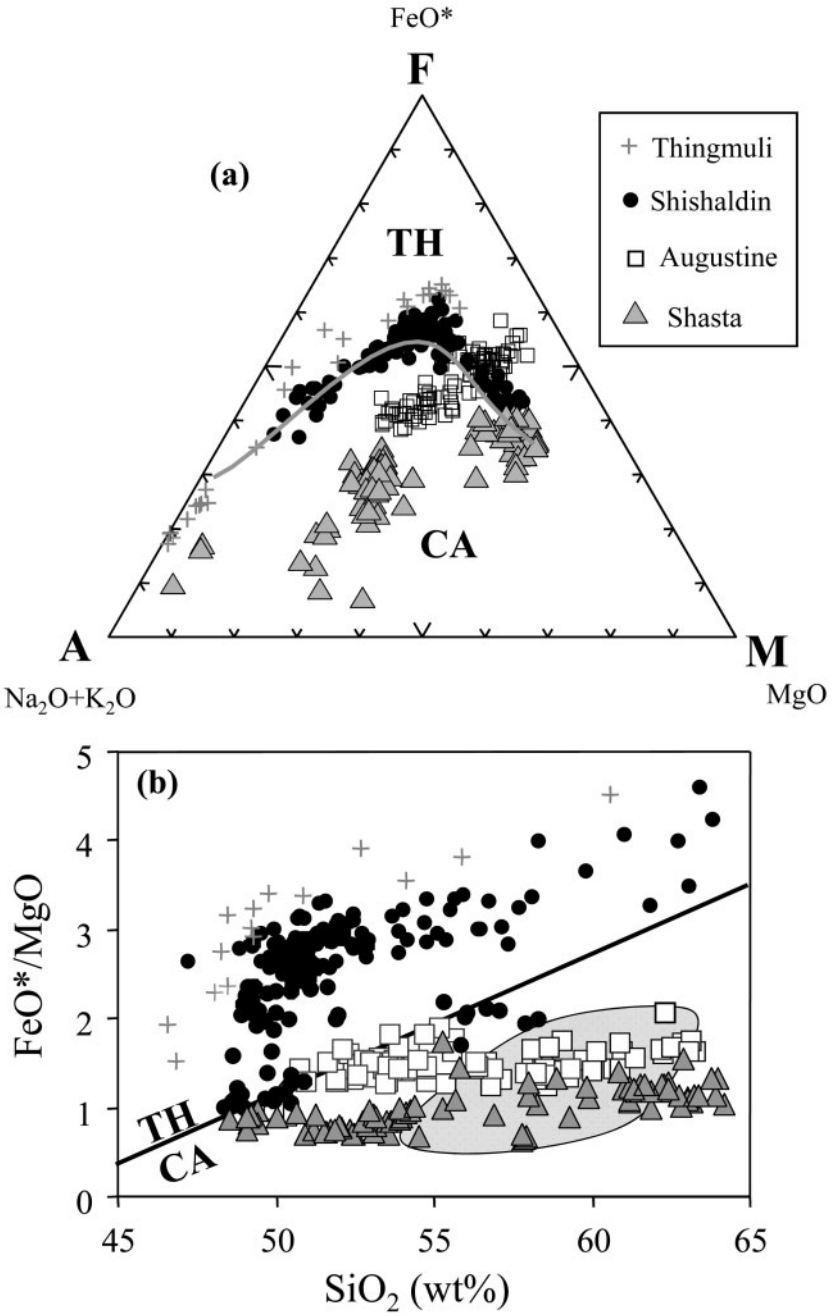

Fig. 1. Discrimination diagrams for tholeiitic (TH) and calc-alkaline (CA) magma series. (a) AFM diagram with dividing line from Irvine & Baragar (1971; continuous gray line) and various volcanic suites: Thingmuli, Iceland (Carmichael, 1964); Shishaldin, Aleutian arc (P. Stelling & C. J. Nye, unpublished data; Fournelle, 1988; this study); Augustine, Aleutian arc (Daley, 1986; Johnson *et al.*, 1996; this study); Shasta, Cascadia (including high-magnesium andesites; Baker *et al.*, 1994; Grove *et al.*, 2001). (b) FeO*/MgO vs SiO_2 discrimination diagram with dividing line from Miyashiro (1974), with the same suites as shown in (a) and high-Mg-number andesites from the Setouchi volcanic belt, Japan (Shiraki *et al.*, 1991), shown as a gray field.

Existing TH and CA classification schemes

Various geochemical diagrams have been developed to describe TH vs CA evolution. On an Alkali–FeO*–MgO (AFM) diagram, a TH magmatic suite evolves toward the FeO* apex before eventually enriching in the alkalis and evolving toward the alkali apex (e.g. Shishaldin volcano and Thingmuli, Fig. 1a). A CA magmatic suite plots on a trend through the middle of the ternary, toward the alkali apex, without showing a trend toward FeO*

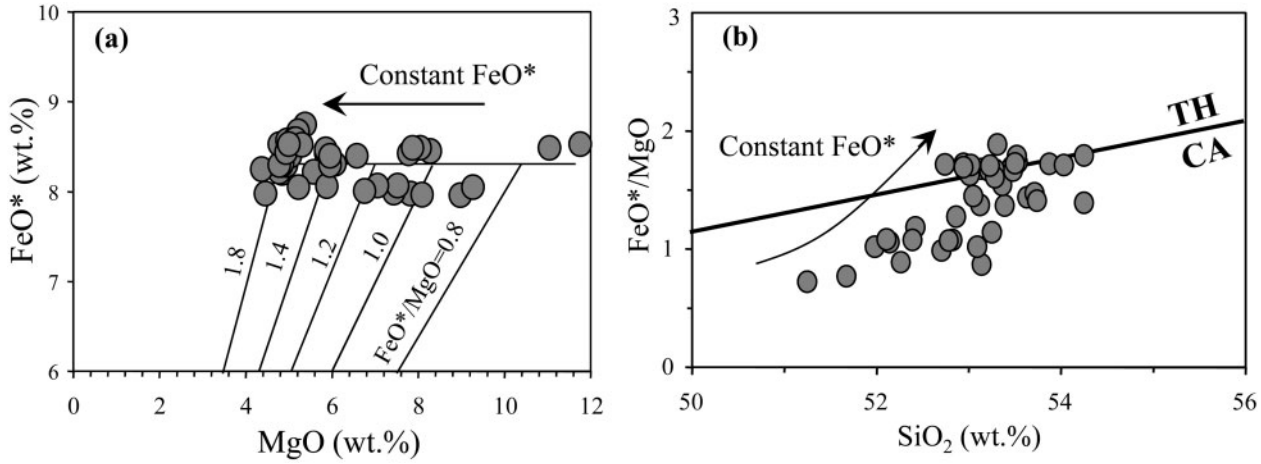

Fig. 2. Data from Klyuchevskoy volcano (gray circles) illustrating differing interpretations possible on two diagrams. The MgO vs FeO* diagram (a) illustrates that the liquid line of descent progresses at constant FeO*, whereas the FeO*/MgO (b) ratio increases. This creates the false impression of Fe enrichment on the FeO*/MgO vs SiO_2 diagram. Despite constant FeO*, FeO*/MgO increases and the magma evolves from the CA to the TH field. After Arculus (2003). Data from Kersting & Arculus (1994).

(e.g. Augustine and Shasta volcanoes, Fig. 1a). Although the AFM diagram is effective in illustrating Fe enrichment in terms of FeO* and MgO components, the inclusion of the alkalis is problematic. For example, Augustine volcano displays a CA trend (Fig. 1a), but its low alkali content (0·5 wt % K_2O for Augustine vs 2 wt % for Shishaldin) places the least evolved compositions well into the TH field. Gill (1981) noted that K_2O varies more than other major elements within andesites from different tectonic settings, and such variations are due in part to different mantle sources and different extents of partial melting. Such primary variations can overwhelm magmatic evolutionary trends and lead to systematics on the AFM diagram that are unrelated to Fe enrichment. In addition, the AFM diagram does not provide a quantitative measure of the extent to which magmas are TH or CA. There is no significance assigned to a magmatic suite plotting significantly above or below the TH–CA dividing line, or how steep or shallow the trend is toward FeO*. Although the AFM diagram shows Fe enrichment, the variation of alkalis and the lack of quantifiable Fe enrichment make the diagram difficult to use to test models for the origin of TH and CA trends.

There are similar ambiguities in the use of the FeO*/MgO–SiO_2 plot (Fig. 1b) of Miyashiro (1974). Its popularity results in part from the simple, linear division between TH and CA regions, for which Miyashiro provided an equation: SiO_2 (wt %) = 6·4 × (FeO*/MgO) + 42·8. This equation was admittedly arbitrary, serving to divide the magmatic suites discussed in the original study (the Skaergaard intrusion, Izu–Bonin, Tonga, Kermadec, and NE Japan volcanic arcs). The FeO*/MgO ratio is useful when evaluating olivine–liquid equilibrium because FeO*/MgO of a liquid is related to FeO*/MgO of coexisting olivine by nearly a constant factor (K_D ~0·3; Roedder & Emslie, 1970; Ford *et al.*, 1983). Thus, a magma in equilibrium with the mantle (≥Fo_{89} olivine) will have FeO*/MgO ≤ 0·73. However, it is problematic to use FeO*/MgO to describe magmatic evolution because absolute FeO* and MgO concentrations may evolve independently. Increasing FeO*/MgO may result from increasing FeO* or decreasing MgO, or from magmas with no absolute enrichment in FeO*. Figure 2 shows an example of decreasing MgO at constant FeO* and the resulting increase in FeO*/MgO. Such a magmatic series might be classified as TH, despite the fact that the magmas do not enrich in FeO*. Hence FeO*/MgO obscures the recognition of processes affecting FeO* evolution along a magma's liquid line of descent.

An additional complexity with the FeO*/MgO–SiO_2 diagram is the use of SiO_2 on the abscissa. Silica dominates the major element budget of most magmas, but variations in SiO_2 may result from magma generation processes, independent of how a magma subsequently evolves. For example, melts of subducted oceanic crust can be andesitic (Tatsumi, 1981; Rapp & Watson, 1995), as can the reaction products of basaltic melt and upper mantle (Kelemen, 1990; Grove *et al.*, 2003), and both types of magma commonly originate in the CA field. Other processes that increase the primary SiO_2 content of a magma include mantle melting at low pressures (Kushiro, 1972; Albarède, 1992; Rogers *et al.*, 1995; Lee *et al.*, 2009), equilibration of melt with harzburgite (Parman & Grove, 2004; Grove *et al.*, 2005), high-pressure fractionation in the presence of garnet (Macpherson *et al.*, 2006), and low-degree melting of H_2O-bearing peridotite (Baker *et al.*, 1995; Gaetani &

Grove, 1998; Hirschmann *et al.*, 1998). Such processes are thought to generate several types of silicic primary magma, including adakites, high-Mg-number andesites, high-Mg-number granitoids (sanukitoids), and boninites (Kay, 1978; Tatsumi & Ishizaka, 1981; Kelemen *et al.*, 1990; Yogodzinski *et al.*, 1994; Falloon & Danyushevsky, 2000; Martin *et al.*, 2005), and most of these will originate in the CA field, independent of how they evolve. Lastly, the silica content of anhydrous or degassed compositions commonly plotted on such diagrams may be artificially raised if the magma contains several wt % H_2O, as a result of the disproportionate effect on silica of closing major element analyses to 100%. Thus, although the FeO*/MgO–SiO_2 diagram may be useful in identifying primary silica variations, this too complicates the isolation of Fe variations, and obscures the distinction between magma generation and evolution. It is also difficult to discern processes affecting Fe enrichment in primitive compositions using FeO*/MgO–SiO_2 because changes in absolute concentrations of FeO* and MgO can occur over very small changes in SiO_2.

There have been some attempts to quantify the extent to which a magma is TH or CA on the Miyashiro diagram. Arculus (2003) concluded a recent review of the issues of 'CA' nomenclature with a suggestion of delineating fields of high-, medium-, and low-Fe on a plot of FeO*/MgO–SiO_2. More recently, Hora *et al.* (2009) proposed a new CA/TH index based on the slope on this diagram. Although such quantification is an improvement, issues remain with interpreting the FeO*/MgO ratio and deconvolving primary silica variations.

THE THOLEIITIC INDEX (THI)

Our goal here is to develop a simple tool for quantifying the extent of Fe enrichment that a magmatic suite experiences during crystallization. Many of the previous efforts described above focused on where magmas plot within certain discriminating fields, whereas we are more interested in how magmas evolve and how to quantify the crystallization paths they take. Toward this end, we propose a new index of Fe enrichment, the Tholeiitic Index (THI). The THI is based on absolute concentrations of FeO* vs MgO:

$$\mathrm{THI} = \mathrm{Fe}_{4\cdot0}/\mathrm{Fe}_{8\cdot0} \quad (1)$$

where $Fe_{4\cdot0}$ is the average FeO* concentration of samples with 4 ± 1 wt % MgO, and $Fe_{8\cdot0}$ is the average FeO* concentration at 8 ± 1 wt % MgO along a given liquid line of descent (LLD). The THI is simply the factor of enrichment or depletion in FeO* as a magma evolves from parental compositions at 8% MgO to more fractionated compositions at 4% MgO. At ≥ 8 wt % MgO, olivine crystallization from basaltic liquid drives relatively little variation in FeO* (Langmuir & Hanson, 1980), and most natural LLDs have initial FeO*–MgO slopes consistent with olivine-dominated crystallization. Thus $Fe_{8\cdot0}$ approximates a magma's primary FeO* concentration. The choice of FeO* at 4 wt % MgO is more arbitrary, and reflects a compromise between an MgO value that is low enough to capture sufficient Fe variation and one that is high enough to avoid the dominance of factors such as crustal assimilation and magma mixing that cause LLDs to converge. The advantage of the THI is that it isolates the evolution of Fe independently of primary magma composition ($Fe_{8\cdot0}$) or other chemical components (e.g. silica or alkalis). The THI quantifies the mode of magma evolution in the early part of its path, as magmas evolve from basaltic to low-silica andesitic compositions.

There are a number of limitations to such an approach to quantify a magmatic LLD. Most of the data in the literature are whole-rock analyses, but a whole-rock is not necessarily a good approximation to a magmatic liquid (e.g. Eichelberger *et al.*, 2006). Processes including crystal accumulation, partial segregation, and filter pressing may result in divergence of whole-rock compositions from true liquids (Sisson & Bacon, 1999). Not only have we used whole-rock samples to approximate the LLD, but we have usually combined all data from a single volcano. Ideally, the THI would be calculated for liquids from single eruptive episodes, but in most cases, too few of such data exist to calculate a meaningful THI. Future work may exploit improvements in the volcanic datasets as more data become available on magmatic liquids (e.g. melt inclusions and aphyric rocks), for multiple eruptions from a single volcano. Despite the limitations of the current global dataset in these ways, there are still large variations in THI to examine regionally and globally.

One advantage of the THI is that it describes the continuum of Fe enrichment observed in natural samples, eliminating the need for further terminology. However, we recognize that the terms 'TH' and 'CA' are deeply embedded in the literature; thus TH and CA are defined here based on the THI. Magma suites that are tholeiitic enrich in Fe and thus have THI > 1; magma suites that are calc-alkaline deplete in Fe and have THI ≤ 1. Although the THI does not include Bowen's original notions regarding silica enrichment, nor subsequent inferences based on the rate of silica enrichment, $Fe_{4\cdot0}$ encompasses a range of compositions, from 50 wt % SiO_2 (basalt) to 56 wt % SiO_2 (low-silica andesite), which includes a major fraction of the magmas erupted on Earth.

We illustrate the utility of the THI by examining its variation in several magmatic suites from different tectonic settings, including 41 magmatic suites from arcs, back-arc basins, mid-ocean ridges (mid-ocean ridge basalt; MORB), ocean islands (ocean island basalt; OIB), and the alkaline volcanoes Etna and Vesuvius (Table 1).

Table 1: Tholeiitic index (THI) and average water content (H_2O) for data shown in Fig. 7[1]

Abbrev.	Volcano	$Fe_{4\cdot0}$	$\pm2\sigma$ SE	$Fe_{8\cdot0}$	or max[2]	$\pm2\sigma$ SE	THI	$\pm2\sigma$ SE	H_2O_{ave} (wt %)	±1 s.d.	No. MI[3]	Tectonic setting[4]
AU	Augustine	6·25	0·24	9·62	*	0·48	0·65	0·041	6·35	0·25	19/59	S
EM	Emmons	8·13	0·14	8·40	*	0·42	0·97	0·051	2·40	0·13	5/111	S
SH	Shishaldin	10·98	0·24	9·50		0·26	1·16	0·040	2·03	0·18	10/33	S
AK	Akutan	9·44	0·40	10·07		1·02	0·94	0·103	3·72	0·09	2/39	S
UN	Unalaska	8·21	0·51	9·20		0·38	0·89	0·066	3·03	0·42	4/26	S
OK	Okmok	9·96	0·48	11·10		0·44	0·90	0·056	2·47	0·15	4/35	S
SE	Seguam	7·30	0·38	8·40		0·50	0·87	0·069	3·30	0·33	14/29	S
KO	Korovin	8·02	0·22	10·19		0·41	0·79	0·038	3·74	0·63	5/14	S
KL	Klyuchevskoy	8·16	0·24	8·39		0·07	0·97	0·030	2·68	0·23	5/29	S
TO	Tolbachik	8·84	0·33	9·10		0·48	0·97	0·063	2·69	0·18	8/11	S
KS	Ksudach	9·08	0·57	9·55	*	0·95	0·95	0·112	3·35	0·19	4/4	S
PA	Parcutin	6·84	0·30	8·46	*	0·85	0·81	0·088	3·29	0·66	5/26	S
FG	Fuego	8·65	0·11	11·01		0·51	0·79	0·038	5·24	0·72	5/28	S
CN	Cerro Negro	9·68	0·21	10·61		0·20	0·91	0·026	5·08	0·72	17/56	S
AR	Arenal	7·22	0·12	9·19	*	0·92	0·79	0·080	3·43	0·48	7/19	S
IZ	Irazú	6·79	0·18	8·04		0·13	0·84	0·026	2·66	0·56	4/11	S
AG	Agrigan	10·00	0·71	11·66	*	1·17	0·86	0·105	4·59	0·55	3/8	S
SA	Sarigan	7·24	0·41	9·16		0·57	0·79	0·067	5·61	0·74	2/4	S
ST	Shasta	4·35	0·14	7·08		0·50	0·61	0·048	8·00[5]	0·80	9/15	S
SI	Satsuma Iwojima	8·97	0·59	9·52	*	0·95	0·94	0·113	2·45	0·31	6/21	S
SR	Stromboli	7·18	0·13	7·72		0·22	0·93	0·031	2·83	0·36	22/23	S
ET	Etna	7·99	0·16	9·58		0·12	0·83	0·020	2·63	0·66	74/101	I
VE	Vesuvius	6·61	0·54	7·30		0·38	0·91	0·088	1·97	0·34	18/44	I
MT	Mariana Trough	10·95	0·59	7·82		0·17	1·40	0·081	1·36	0·42	44/66	B
LB	Lau Basin[6]	11·24	0·25	9·03		0·21	1·24	0·040	1·18	0·73	24/56	B
CL	Lau Basin - CLSC[7]	16·44	0·21	9·14		0·32	1·80	0·067	0·52	0·27	6/24	B
MB	Manus Basin	12·74	1·04	10·15		0·59	1·26	0·125	0·74	0·39	27/52	B
SC	E. Scotia Ridge	10·15	0·34	8·17		0·22	1·24	0·054	1·05	0·50	6/73	B
WB	Woodlark Basin	12·52	1·01	8·94		0·33	1·40	0·124	0·32	0·05	14/16	B
FJ	N. Fiji Basin	10·98	0·72	9·57		0·12	1·15	0·077	0·81	0·54	14/19	B
GL	Galapagos	16·08	0·72	10·04		0·17	1·60	0·077	0·31	0·21	35/42	M
ER	East Pacific Rise	15·68	0·66	9·89		0·27	1·59	0·079	0·25	0·08	26/26	M
IR	SE Indian Ridge	13·19	0·10	8·58		0·31	1·54	0·057	0		-	M
SM	Samoa	12·48	0·26	11·40		0·29	1·09	0·036	1·24	0·12	40/94	O
RE	Reunion	12·34	1·32	11·50		0·10	1·07	0·231	0·76	0·12	24/29	O
HK	Hekla	13·91	0·71	12·58		0·65	1·11	0·161	1·07	0·90	4/4	O
HKi	Hawaii: Kilauea	13·00	0·07	11·22		0·06	1·16	0·009	0·40[8]	0·04		O
HMk	Hawaii: Mauna Kea	10·61	0·10	11·52		0·09	0·92	0·011	0·36[8]	0·04		O
HMl	Hawaii: Mauna Loa	14·96	0·37	10·80		0·06	1·39	0·035	0·36[8]	0·04		O
Hko	Hawaii: Koolau	11·48	1·08	10·56		0·09	1·09	0·102	0·40[8]	0·04		O
HLo	Hawaii: Loihi	12·35	0·37	11·44		0·20	1·08	0·038	0·48[8]	0·05		O
TH	Thingmuli	13·81	0·66	11·51	*	1·15	1·20	0·133	-	-	-	LM
SK	Skaergaard	21·64	2·24	15·09		3·00	1·43	0·321	-	-	-	LM

[1]THI = $Fe_{4\cdot0}/Fe_{8\cdot0}$. $Fe_{4\cdot0}$ is the average FeO* for compositions with 3–5 wt % MgO; data are binned in 0·5 wt % MgO intervals, and the average of these four bins is taken as $Fe_{4\cdot0} \pm 2\sigma$ standard error of the mean. $Fe_{8\cdot0}$ = average FeO* from 7 to 9 wt % MgO, calculated in the same manner as $Fe_{4\cdot0}$. THI error propagated from the 2σ standard deviation of the mean of $Fe_{4\cdot0}$ and $Fe_{8\cdot0}$. (See Electronic Appendix A for whole-rock and melt inclusion or glass references, and details on calculations for each suite.)
[2]For volcanoes where $Fe_{8\cdot0}$ is constrained by one value (or max), error on $Fe_{8\cdot0}$ is assumed to be $\pm10\%$.
[3]First value: number of melt inclusions or glasses used to calculate H_2O (wt %); second value: total number of melt inclusions or glasses evaluated. MI that are degassed or have compositions falling off the volcano LLD were excluded from THI and H_2O calculation (see text for details).
[4]S, subduction zone; M, mid-ocean ridge; B, back-arc basin; O, ocean island; I, intraplate volcano; LM, layered mafic intrusion.
[5]Water contents for Shasta derived from experimental data only (Grove *et al.*, 2002). Error assumed to be $\pm10\%$.
[6]Includes data from Eastern Lau Spreading Center (LSC), Intermediate LSC, Mangatolu Triple Junction, Valu Fa.
[7]Includes data from Central LSC only.
[8]H_2O (wt %) from estimated primary water contents based on glass or melt inclusion data (see text): Hauri (2002): Kilauea, Mauna Kea, Mauna Loa, Koolau, Loihi; Davis *et al.* (2003): Kilauea, Mauna Loa, Loihi; Seaman *et al.* (2004): Mauna Kea. Error assumed to be $\pm10\%$.

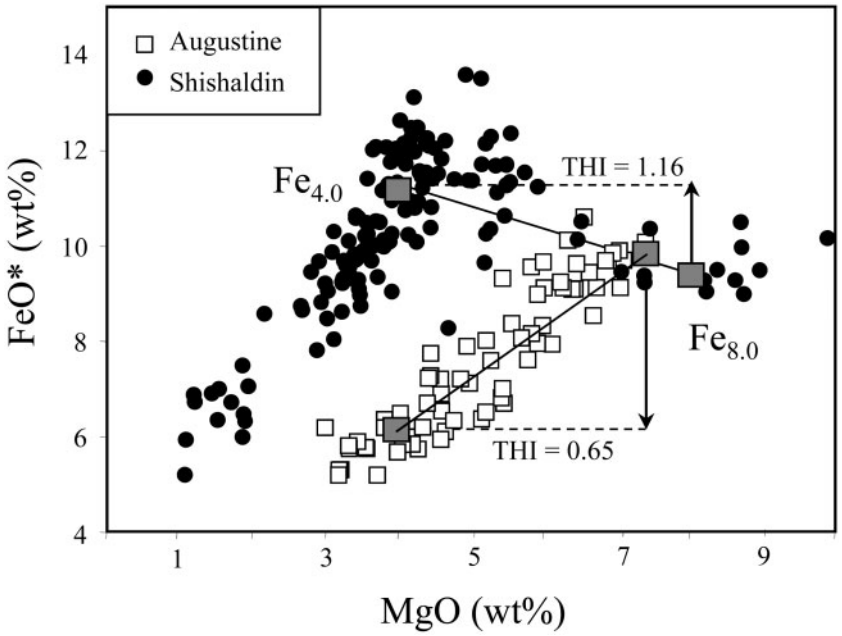

Fig. 3. Calculation of the THI (Tholeiitic Index) = $Fe_{4\cdot0}/Fe_{8\cdot0}$. $Fe_{4\cdot0}$ is the average FeO* concentration of samples between 3 and 5 wt % MgO. If there are sufficient data (as for Shishaldin), $Fe_{8\cdot0}$ is the average FeO* concentration of samples between 7 and 9 wt % MgO; if not, then the sample with the highest MgO is used to approximate $Fe_{8\cdot0}$ (as for Augustine). Shishaldin has a tholeiitic trend (THI > 1); Augustine has a strongly calc-alkaline trend (THI < 1).

We calculate the THI using mostly whole-rock and some melt inclusion data from the literature and this study, making substantial use of the GEOROC database (http://georoc.mpch-mainz.gwdg.de/georoc/) and PetDB (http://www.petdb.org/petdbWeb/index.jsp). Details on the data type and references for each volcanic suite can be found in Electronic Appendix A (available at http://www.petrology.oxfordjournals.org). When abundant analyses are available, the data are binned in 0·5 wt % MgO intervals, and the four bins between 7 and 9 wt % MgO are averaged to obtain $Fe_{8\cdot0}$. A similar procedure is used to obtain $Fe_{4\cdot0}$. Uncertainties in THI are calculated by propagating the 2σ standard error of the mean for $Fe_{4\cdot0}$ and $Fe_{8\cdot0}$ onto their ratio (Table 1). Unfortunately, many arc volcanoes in particular do not erupt magmas with >7 wt % MgO, or those with >7 wt % MgO may reflect olivine and/or clinopyroxene accumulation. In these cases, the FeO* content of the samples with the highest MgO was used to estimate $Fe_{8\cdot0}$, provided a suite had at least one sample with ≥6 wt % MgO. We also discovered many examples of reporting errors, where Fe_2O_3 has been reported as FeO, or vice versa. Such issues are pervasive in the global dataset, and we have contacted original authors in some cases to rectify the issue but suspect that many cases have gone undetected. These issues introduce additional errors in the estimation of THI from the global dataset. In addition, other methods of calculating $Fe_{4\cdot0}$ and $Fe_{8\cdot0}$ were also examined, including extrapolating to $Fe_{8\cdot0}$ for volcanic suites with sparse data >6 wt % MgO, or by regressing the data to calculate $Fe_{4\cdot0}$ and $Fe_{8\cdot0}$. For the Aleutians, these other methods resulted in very little change in the THI, with the differences generally falling within the reported error of the THI. Thus we have chosen to calculate THI using binned averages for the Aleutians and all other suites examined here. Provided the treatment of the data and error propagation are robust, however, such alternative methods of calculating $Fe_{4\cdot0}$ and $Fe_{8\cdot0}$ are acceptable.

As an example of the efficacy of the THI, Fig. 3 illustrates MgO and FeO* variations in Shishaldin and Augustine volcanoes in the Aleutians, which span the global array of arc TH and CA evolutionary trends (Table 1). Shishaldin volcano has the highest THI of 1·16, indicating that FeO* has enriched by 16% from 8 to 4% MgO. The THI clearly underestimates Fe enrichment in this case, which is as high as 1·4 at ~5% MgO, when magnetite fractionation starts to affect the LLD. Although it would be preferable to account for such features in each LLD, such inferences become difficult for suites with few data, and so we have chosen a consistent measure such as $Fe_{4\cdot0}$. Despite these issues, the THI for Shishaldin classifies it as one of the most tholeiitic arc suites, consistent with its placement on the traditional AFM and FeO*/MgO–SiO_2 diagrams (Fig. 1). At the other extreme, Augustine volcano has a THI of 0·65, indicating 35% depletion in FeO* at 4% MgO. Augustine is thus strongly CA,

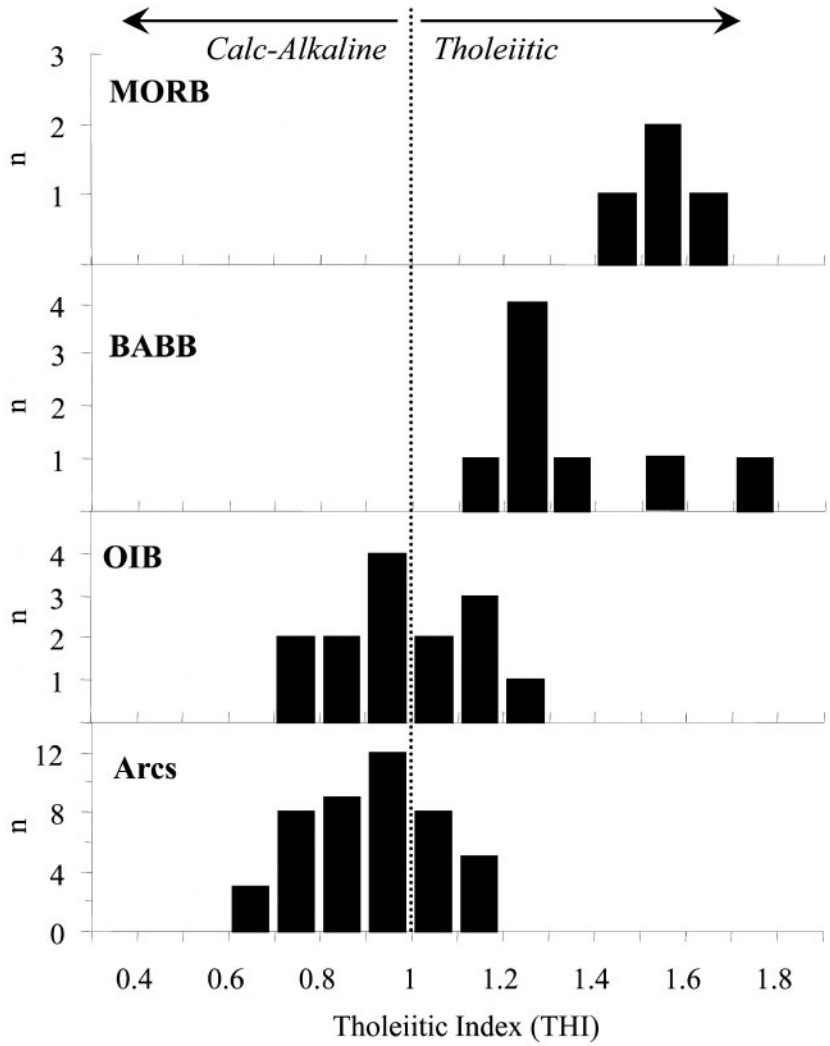

Fig. 4. Histograms showing the range in THI for magmatic suites from various tectonic settings. Most data are in Table 1 (see references in Electronic Appendix A). MORB, mid-ocean ridge basalt; BABB, back-arc basin basalt; OIB, ocean island basalt.

consistent with where most of the data plot on the traditional diagrams. Thus, THI discriminates strongly between these two volcanoes of the Aleutian arc and provides a quantitative measure of their Fe evolution that can be tested against intensive variables (e.g. water, pressure, composition, fO_2) and predictions from petrological models.

Figure 4 compares the THI for volcanic suites from different tectonic settings. Few MORB suites evolve to 4% MgO, but those that do have a high THI (>1·4), and are strongly tholeiitic. Eight back-arc spreading segments include compositions with 4% MgO; some overlap in their THI with MORB, but most extend to lower values (THI = 1·14–1·80). Ocean island and volcanic arc suites show the largest variations in THI and range from TH to strongly CA trends. Thus, the THI discriminates effectively between magmas from different tectonic settings, with all MORB and back-arc volcanic suites being TH, and some OIB and most arc suites being strongly CA. TH magmas are found in all tectonic settings, but most arc volcanoes are CA. The THI thus conforms to the common notions and usage of the terms tholeiitic and calc-alkaline.

In summary, the THI quantitatively describes the continuum of Fe enrichment in magmas (Miyashiro, 1974) and improves upon other terms such as 'transitional' (Kay & Kay, 1985) and 'high-, medium-, and low-Fe' (Arculus, 2003). The THI effectively discriminates some of the major magma series on a global basis, not just within subduction zones, with THI decreasing on average from MORBs to back-arc basin basalts to OIB to arc magmas. Most importantly, the THI allows quantitative tests of hypotheses for the origin of TH and CA magma series.

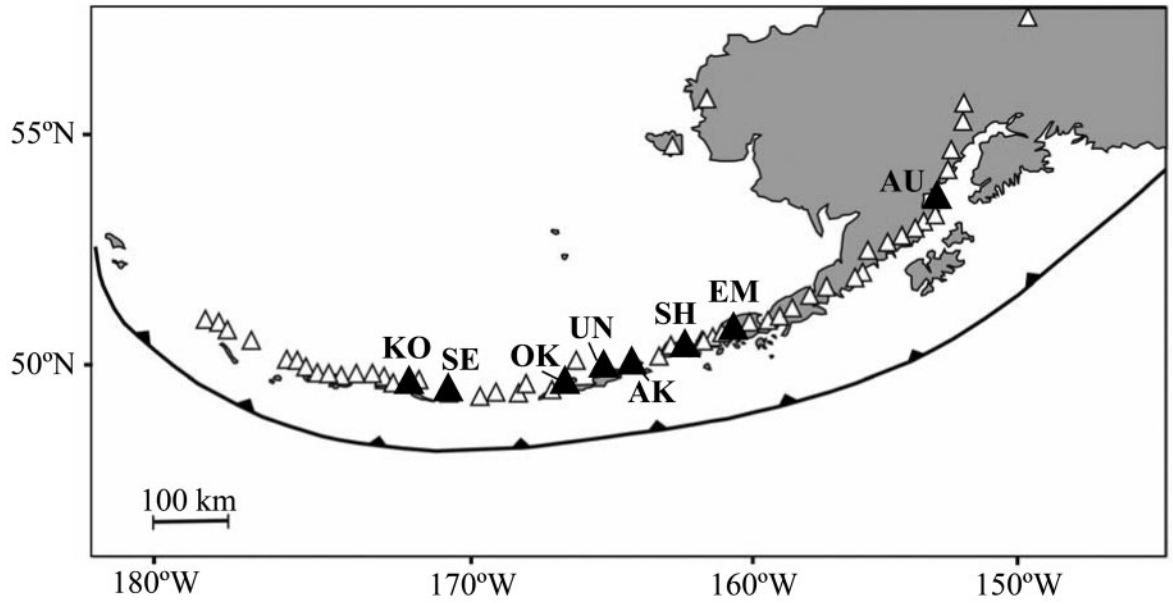

Fig. 5. Alaska–Aleutian volcanic arc, resulting from convergence between the Pacific and North American plates. Volcanoes shown as triangles; black triangles denote volcanoes with melt inclusion data reported in this study. AU, Augustine; EM, Emmons; SH, Shishaldin; AK, Akutan; UN, Unalaska Island (including Pakushin and Angela's Cone); OK, Okmok; SE, Seguam; KO, Korovin.

Generating calc-alkaline fractionation trends

The benefit of developing a new index of Fe enrichment is not only to improve upon the ambiguities with current classification schemes for igneous rocks, but to shed light on their origins. Tholeiitic magma series, as observed ubiquitously at mid-ocean ridges, are well reproduced with both laboratory and thermodynamic simulations of crystal fractionation of dry magma at low pressure (Grove & Bryan, 1983; Langmuir *et al.*, 1992). Dry basaltic liquids at low pressure generally crystallize olivine first, which has little effect on FeO*. Plagioclase is typically the next phase on the cotectic, which both retards the rate of Mg depletion and accelerates the rate of Fe enrichment per increment crystallized. The appearance of plagioclase typically coincides with the onset of strong Fe enrichment and tholeiitic differentiation.

Conversely, there are many ways to generate a CA trend of Fe depletion. These involve, logically, the suppression of plagioclase crystallization as a result of (1) high water content (Grove & Baker, 1984; Baker & Eggler, 1987; Kinzler & Grove, 1992; Sisson & Grove, 1993*a*; Grove *et al.*, 2003), (2) high pressure of crystallization (Baker & Eggler, 1987; Gust & Perfit, 1987; Kinzler & Grove, 1992), or (3) bulk composition (variations in CaO/Al_2O_3, Na_2O/Al_2O_3, and FeO*; Grove & Baker, 1984; Miller *et al.*, 1992). Other long-standing theories for generating CA trends involve the early crystallization of Fe-rich phases, such as magnetite, which requires high oxygen fugacity and/or H_2O (Osborn, 1959; Gill, 1981; Sisson & Grove, 1993*a*, 1993*b*), and amphibole, which requires high H_2O and Na_2O (Cawthorn & O'Hara, 1976; Grove *et al.*, 2003). Assimilation and mixing with low-Fe silicic melts (Grove & Baker, 1984; McBirney *et al.*, 1987; George *et al.*, 2004) or mantle–melt reaction (Kelemen, 1990) may also create a CA trend.

Of each of these controls, magmatic water content has long figured prominently in the theories for CA evolution because it can drive CA differentiation in three independent ways: by suppressing plagioclase, enhancing magnetite, and permitting amphibole crystallization. Yet until recently, measurements of pre-eruptive water contents have been scarce and inconsistent, largely because all volcanic rocks degas as they reach the surface where we sample them. Recent developments in microanalysis [Fourier transform infrared spectroscopy (FTIR) and secondary ionization mass spectrometry (SIMS)] and successful application to quenched glasses and melt inclusions have produced a rapidly expanding database of water measurements in magmas from subduction zones, mid-ocean ridges, back-arc basins, and ocean islands. For this reason, we focus this study on the role of water in generating the CA trend, and we present new data for the water contents of magmas from Aleutian volcanoes that possess large variations in THI (Table 1, Fig. 5). After presentation of the new data, we return to assess the quantitative role of water in driving differentiation in arc magmas.

SAMPLES AND METHODS

Melt inclusion (MI) data were collected from eight volcanoes in the Aleutian–Alaskan volcanic arc: Augustine, Emmons, Shishaldin, Akutan, Makushin, Okmok, Seguam, and Korovin (Fig. 5). Great effort was made to obtain fresh, small-diameter mafic tephra (<2 cm lapilli), as this material has cooled rapidly and preserves the glassiest MIs with the highest volatile contents. Samples from Pakushin and Angela's Cone (flank cones of Makushin volcano on Unalaska Island), Akutan volcano, and Pyre Peak of Seguam Island were collected during dedicated field campaigns in 2005 and 2007, with sample numbers prefaced by 05MZPK-, 05EHPK-, 05AKTAP-, and SEG-07- (see further sample details and locations in Electronic Appendices B and C; http://www.petrology.oxfordjournals.org). Many other samples were donated generously by the Alaska Volcano Observatory and the Plate Boundary Observatory, as well as by scientists from other institutions (especially A. Anderson and R. Kay). Although samples from historical eruptions were preferred, samples are at most Holocene in age (see below). We sought olivine-hosted MIs from mafic scoria because these MIs are the most relevant for the part of the LLD relevant to the THI (i.e. 8 to 4% MgO), where olivine is an early and major phase. Some plagioclase- and pyroxene-hosted MIs were also analyzed in samples ranging from basalt to andesite in composition.

Whole-rocks: major elements

Bulk-rock samples were analyzed for major elements at Boston University (BU) and Michigan State University. At BU, samples were fused following the techniques of Kelley *et al.* (2003) and Wade *et al.* (2006). Samples were crushed in an alumina jaw-crusher, hand-picked to avoid weathered surfaces, sonicated, dried at <100°C, and powdered in an alumina ball mill. For major elements, powders were fused with $LiBO_2$ then dissolved in nitric acid, and finally diluted to ~4300 × dilution of the original sample. The solutions were analyzed for 10 major elements and seven trace elements by inductively coupled plasma atomic emission spectrometry (ICP-AES) using a Jobin-Yvon 170C system. Whole-rock samples from Okmok and Seguam were analyzed by X-ray fluorescence (XRF) at Michigan State University following the protocol of Vogel *et al.* (2006). Glass disks were fused using lithium tetraborate flux and ammonium nitrate to enhance oxidation during fusion. Fused disks were then analyzed for major elements and three trace elements (Rb, Sr, Zr) on a Bruker S4 Pioneer XRF system. Data were reduced using fundamental parameters in SPECTRAplus software (Bruker AXS, Germany) on the S4 Pioneer; trace elements were determined using linear regression of external standards. Precision for most elements is <1% RSD, except for P_2O_5 (<2%). Only major element data are reported for whole-rocks (Electronic Appendix D; http://www.petrology.oxfordjournals.org); trace element data will be presented elsewhere.

Melt inclusions: major elements and volatiles

To extract MI-bearing phenocrysts, tephra samples were crushed with an alumina jaw crusher or steel percussion mortar and sieved. Olivine-, plagioclase-, and pyroxene-hosted MIs were hand-picked from sieved aliquots ranging in size from 150 to 1000 μm. We were highly selective in picking MIs for analysis, selecting only glassy inclusions lacking cracks, breaches, daughter crystals or devitrification textures, and avoiding inclusions in contact with the exterior of the host phenocryst. We did not heat, homogenize, or treat the MIs in any way, except for some phenocrysts from Angela's Cone. As a result of extreme alteration, the exterior of olivine phenocrysts from Angela's Cone had an orange tint. After observing contamination of the MI surface during SIMS analysis (e.g. CO_2 decrease and H_2O increase with continued sputtering), some phenocrysts (05MZPK-09.oliv5-10) were soaked in a 2N HCl bath for 20 min to prevent the altered material from smearing onto the exposed surface during polishing. Although contamination was generally avoided by pre-sputtering (see below), the length of time for the contamination signal to disappear was significantly reduced in the MIs treated with HCl. Melt inclusions and host phenocrysts from each volcano were polished and mounted in indium metal, which minimizes background volatile counts in the ion probe (Hauri *et al.*, 2002). Melt inclusions from Emmons volcano were either mounted in indium metal or mounted in holes drilled into a brass ring and back-filled with epoxy.

The volatiles H_2O, CO_2, S, Cl, and F were analyzed by SIMS (Electronic Appendix E; http://www.petrology.oxfordjournals.org) at the Carnegie Institution of Washington with a Cameca 6f ion microprobe during six sessions. Inclusions were analyzed following the protocol of Hauri *et al.* (2002), using an 8 nA beam current, 30 μm spot size, and 5 keV accelerating voltage. On-peak count times were ~5 s. Prior to each analytical session, glass standards with known volatile concentrations were analyzed to generate calibration curves, with no explicit correction for Si. Water was measured as ^{1}H or $^{1}H^{16}O$. Precision during the sessions was 5% 1σ for H_2O and CO_2, and 6% 1σ for F, S, and Cl based on replicate analyses of our melt inclusions and standard glasses. Precision between multiple sessions was ~10% for all volatile species (Cooper, 2009).

Major element, S, and Cl concentrations were determined by electron microprobe analysis (EPMA) on a JEOL JXA-733 Superprobe at the Massachusetts Institute of Technology (MIT) or on a Cameca SX 100 EPMA at the American Museum of Natural History (AMNH;

Electronic Appendix E). On the MIT microprobe, samples were analyzed using a 10 nA beam current, 10 μm spot, and 15 keV accelerating voltage. Elements were counted for 40 s with the exception of Na, which was counted for 5 s. At the AMNH, F was analyzed in addition to the other elements. Major elements were analyzed using a 10 nA beam current, 12 μm spot size, and 15 keV accelerating voltage. Volatile elements S, Cl, and F were analyzed using a 40 nA beam current, 12 μm spot size, and 15 keV accelerating voltage. Counting times vary by element: 20 s for Na, K, Al, Ca, Mg, Fe, Mn, P, and Ti; 30 s for Si; 120 s for F; and 140 s for S and Cl. Uncertainty on S and Cl is ≤17% and ≤6%, respectively, at MIT, and ∼3% at AMNH for these sessions. Sulfur and Cl by SIMS and EPMA generally agree, but we have noticed a bias of higher S by SIMS, and higher Cl by EPMA (see also Cooper, 2009). Measurements of water contents by SIMS agree with estimations of water contents by sum-deficit using EMPA major element totals, with an average absolute difference of 1·3 wt %. The largest deviations (up to 7 wt %) result for the more hydrous glasses (e.g. Augustine, >7 wt % H_2O), where problems with alkali loss and water by difference estimations are greater (Devine *et al.*, 1995). Although we minimized counting times and/or analyzed alkalis first to minimize alkali loss, analyses from one session were affected by significant alkali loss and are noted with an asterisk after the sample ID in Electronic Appendix E. Water and S data illustrated and used in calculations are derived from the SIMS measurements and supplemented with electron microprobe measurements when SIMS data were unavailable.

Sulfur speciation was determined by wavelength-dispersive sulfur Kα scans (SKα) on the AMNH microprobe on a small subset of the melt inclusions (generally those with abundant S concentrations), following the techniques of Wallace & Carmichael (1992) and Carroll & Rutherford (1988), and the protocol of Mandeville *et al.* (2009). FeS and $BaSO_4$ were analyzed using a 40 nA current, 12 μm spot size, and 15 keV accelerating voltage. Eight to 16 continuous S X-ray scans were carried out for each MI, and the beam was moved every four scans to avoid oxidation of the glass (Wallace & Carmichael, 1992; Métrich & Clocchiatti, 1996). Oxygen fugacities were then calculated using the sulfur speciation model of Wallace & Carmichael (1994) and are reported in Electronic Appendix G (http://www.petrology.oxfordjournals.org) and summarized in Table 2. Based on a duplicate measurement of the same melt inclusion in separate sessions, as well as replicates on the sulfide and sulfate standard materials, we estimate uncertainty on fO_2 from the SKα shifts of ±0·3 log units.

Table 2: Summary of oxygen fugacity, THI, and H_2O for volcanoes in Fig. 9

Volcano	THI	H_2O (wt %)[1]	fO_2 (ΔFMQ)[2]	fO_2 refs[3]
Augustine	0·65	6·35, 5·39	1·4, 2·1	this study, 1
Emmons	0·97	2·40	1·0	this study
Shishaldin[4]	1·16	2·03	1·8	this study
Akutan	0·94	3·72	1·4	this study
Seguam	0·87	3·30	1·2	this study
Korovin	0·79	3·74	1·5	this study
Paricutin	0·81	3·29	0·7	1
Cerro Negro	0·91	5·08	0·2	2
Arenal	0·79	3·43	1·6	3
Irazu	0·84	2·66	1·3	4
Sarigan	0·79	5·61	1·6	1
Galunggung, Java[5]	1·29	0·26	0·16	1
Barren Island, Andaman	n.d.	4·00	0·96	1
Stromboli	0·93	2·83	0·5	5
Mariana Trough	1·40	0·5 to 1·89	−0·04 to 0·46	1
Lau Basin—CLSC[6]	1·80	0·52	−0·7, −0·9	6, 7
Galapagos	1·60	0·31	−0·3	8
SE Indian Ridge	1·54	n.d.	−1·2	8
East Pacific Rise	1·59	0·25	−0·14 to −0·24	1
JDF Ridge	n.d.	0·73	0·06	1
Kilauea	1·16	0·40	−0·6	8

A more detailed table is given in Electronic Appendix G. n.d., not determined (not enough data for THI calculation or no measured H_2O).
[1]For samples from Kelley & Cottrell (2009) (ref. 1), H_2O determined by SIMS or FTIR and reported as in their study.
[2]For Kelley & Cottrell (2009) data (ref. 1), fO_2 calculated at 1100°C and 1 kbar from $Fe^{3+}/\sum Fe$ measurements using relationship of Kress & Carmichael (1991).
[3]References: 1, Kelley & Cottrell (2009); 2, Sutton *et al.* (2005); 3, Wade *et al.* (2006); 4, Benjamin *et al.* (2007); 5, Métrich *et al.* (2002); 6, Nilsson Farley (1994); 7, Wallace & Carmichael (1994); 8, Wallace & Carmichael (1992).
[4]SKα measured on a compromised inclusion; data not included in Fig. 9.
[5]Details for Galunggung THI calculation are given in Electronic Appendix A.
[6]Includes data for Central Lau Spreading Center only.

Phenocrysts: major elements

Major element concentrations of host phenocrysts (olivine, plagioclase, and pyroxene) were determined by electron microprobe at MIT and the AMNH. On the MIT microprobe, samples were analyzed using a 10 nA beam current, 10 μm spot, and 15 keV accelerating voltage, with the following counting times: 60 s for Fe; 20 s for Na, Ca, and Si; 40 s for all other elements. At the AMNH, analytical conditions were the same as for the glasses, with the exception of counting times: 20 s for Na and Al; 30 s for all other elements. Phenocrysts were analyzed, on average,

in 2–3 separate locations, including adjacent to the MI. Analytical results and location of analyses relative to MIs are given in Electronic Appendix F (http://www.petrology.oxfordjournals.org).

RESULTS

New melt inclusion data for Aleutian–Alaskan volcanoes

The data reported here on the volatile contents of Aleutian melt inclusions constitute the first large-scale study of this kind in the Aleutian arc. Thus, we describe in some detail the MI data, their systematics, and their relationship to the magmas erupted from each of the eight volcanoes studied. More detailed descriptions of samples and locations, and the data tables, can be found in the Electronic Appendices B–F. All MIs and whole-rock analyses were normalized to 100% anhydrous for the purpose of calculating the THI.

Complexities of melt inclusions and selectivity criteria

Our goal is to calculate the THI from cogenetic Aleutian magmas and ascribe a water content to each THI from the MI data. This goal is not a simple one to achieve. One set of reasons, as discussed above, relates to whole-rocks not representing liquids, not being cogenetic, or not including compositions near 8% MgO. MIs potentially solve some of these problems, as they are trapped as magmatic liquids and may preserve early, more primitive and undegassed compositions, especially if trapped in olivine. In reality, MIs have many issues as well. Because MIs play a crucial role in determining magmatic water contents, we discuss some of these issues here and how they may affect calculation of the THI.

Several processes may affect the major element composition of the melt and/or host mineral after inclusion entrapment. For example, MIs commonly undergo post-entrapment crystallization, where a thin rim of olivine crystallizes along the mineral–inclusion interface at the expense of the trapped melt (Danyushevsky *et al.*, 2000, 2002). Olivine-hosted MIs that have undergone post-entrapment crystallization generally reflect equilibration with an olivine composition more evolved (lower MgO/FeO) than that measured in the adjacent host. This process is particularly a problem for the THI, as MgO and FeO* are the very elements of interest here. Here we correct for post-entrapment crystallization by adding equilibrium olivine in 1% increments until the MI is in equilibrium with the adjacent olivine host, assuming $K_D^{Fe/Mg} = 0{\cdot}3$ (note that we did not reheat or homogenize Aleutians MIs). For most inclusions, less than 10% olivine was added; only MIs with ≤15% olivine addition were used to calculate THI. For the purposes of these calculations, all Fe was assumed to be Fe^{2+}. Although Fe^{3+} content may be as high as 30% in some melt inclusions (see below), it is constrained in only a small subset of the volcanoes examined here, so we assume $Fe^{2+}/\Sigma Fe$ is unity for the purposes of like comparison. This assumption may lead to overestimation of the extent of post-entrapment olivine crystallization, but because the slope of an olivine-only LLD is fairly shallow, an overestimate of post-entrapment crystallization may have a minimal effect on $Fe_{8{\cdot}0}$.

At slower cooling rates, MIs will diffusively exchange with their crystal hosts, and given enough time, MIs and hosts can completely re-equilibrate with the exterior melt (Danyushevsky *et al.*, 2000; Gaetani & Watson, 2000). In the case of such diffusive exchange during cooling, the MI evolves to lower MgO and FeO* than the original melt, and its composition cannot be restored by simply adding olivine to the MI. Such inclusions are recognized by possessing substantially lower FeO* than the whole-rocks. We have strived to avoid these effects by analyzing MIs from rapidly cooled tephra samples and by excluding those inclusions that deviate strongly from whole-rock trends.

Another major process that affects both the major and volatile elements in MI is degassing. MIs are commonly trapped during ascent, as the magma is losing a significant amount of H_2O, CO_2 and S to vapor, and crystallizing rapidly. Thus at best, MIs record the degassing process, and measured H_2O, S and CO_2 concentrations are always probably less than what was originally dissolved in the primary magma. For the purposes of the THI, we do not seek primary H_2O contents, but instead those that characterize the part of the liquid line of descent between 8 and 4% MgO. MIs trapped late in the degassing process, however, will record a local, interstitial melt composition that reflects lower pH_2O than reflected in the liquid line of descent developed deeper in the system and defined by the whole-rock compositions (Blundy & Cashman, 2005). These MI compositions diverge dramatically from those of the whole-rocks, often plotting at higher FeO* (reflecting the onset of plagioclase crystallization in the degassed groundmass) and are not used to determine the THI.

Finally, even after entrapment, there may be loss of H_2O from the inclusion through the host. Recent work by Portnyagin *et al.* (2008) indicates that the diffusion of molecular water between MIs and the host magma may be as rapid as proton vacancy diffusion in olivine (Mackwell & Kohlstedt, 1990); thus MIs that reside in degassed magma for relatively short periods (hours to days) may have evolved toward this most recent equilibrium state rather than retain the initially trapped H_2O content. The analysis of MIs from rapidly quenched pyroclastic deposits (ash or lapilli), as considered here, is the first safeguard against such water loss, as they cool rapidly enough (minutes) to prevent significant water loss through the olivine.

Clearly, some criteria must be applied to select MIs that have experienced the least amount of water loss and

major element exchange, such that their compositions are relevant to the main magma crystallization path. Some studies have advocated choosing a single MI with the highest water content (Johnson *et al.*, 2009), whereas others have developed a screening criterion based on other more readily degassed volatile species such as CO_2 or S (Kelley *et al.*, 2010). It is difficult to apply such a criterion here because of the very different absolute levels of volatile species in different Aleutian magmas (e.g. S varying from <1000 to >5000 ppm). Thus a careful assessment of the degassing history of each magma is required. Considering the sum of confounding processes above, all prospects are improved by focusing only on the least degassed inclusions: their high water contents attest to deep formation, rapid ascent and cooling, and thus the least time for exchange or crystallization. Least degassed MIs also approach the magma conditions prior to ascent, in the magma storage region where the whole-rock compositions of magmas are largely set.

Thus our strategy in assessing the Aleutian data is to select MIs with the highest H_2O contents, and that also have major element compositions that overlap with the liquid line of descent defined by the whole-rocks. In this way we ensure coherence between the H_2O contents in the MIs and the major element variations that define the THI. We have also found that the MIs with the highest H_2O contents are generally trapped in the olivines with the highest Fo content and probably represent the most primitive liquids, which are most useful for approximating $Fe_{8\cdot0}$.

Despite a clear strategy, the application is not straightforward, as MI and whole-rock populations are variable for every volcano. In several Aleutian volcanoes (see examples below), only MIs with the highest H_2O contents overlap with the whole-rocks, and more degassed and/or evolved MIs diverge dramatically from whole-rock compositions for reasons outlined above. In other cases MIs extend to higher MgO than the whole-rocks, or the most primitive whole-rocks have demonstrably accumulated crystals and do not represent liquids, so using MIs alone allows a more robust calculation of $Fe_{8\cdot0}$. In several other instances, the THI derives from only the whole-rock analyses, and only H_2O derives from the MIs. Thus in practice, the THI was calculated from a mix of MIs and whole-rock compositions that varies for each volcano. Below we discuss how the THI and H_2O are calculated for eight Aleutian volcanoes. As each volcano is examined in detail, two features are emphasized: the degassing history, illustrated by the H_2O–S systematics recorded in MIs, and the MgO–FeO* LLD of both MIs and whole-rocks. Although MgO–FeO* systematics are emphasized here, all major element systematics must be scrutinized for evidence of mixing or other processes that would influence the interpretation of the THI.

H_2O and THI for Aleutian–Alaskan volcanoes

Augustine volcano

The recent and continuing eruptions of Augustine volcano have produced andesitic, dacitic, and occasionally rhyolitic lava domes, debris flows (dome collapses), pyroclastic flows, and rare lava flows (e.g. Roman *et al.*, 2006; Tappen *et al.*, 2009). In contrast, the samples studied here derive from the only outcrop on Augustine volcano that contains basaltic material, variously interpreted as a hyaloclastite or debris flow of Pleistocene age (20 000 years BP; J. Beget, personal communication), or a basal surge deposit (C. Mandeville, unpublished data), on the south flank of the volcano. Several basaltic pyroclasts were picked from the deposit and given separate names (84AU112, 05AUNY10, 05AUNY17). A detailed description of 84AU112 has been given by Daley (1986), but all three clasts are lithologically similar and include the same mineralogy (olivine + clinopyroxene ± hornblende, with extremely rare, possibly xenocrystic, plagioclase). These pyroclasts are notably crystal rich (>40% crystals) and believed to have accumulated phenocrysts, especially clinopyroxene (Daley, 1986). Their major element compositions reflect this process (gray shaded region in Fig. 6a), and do not overlap with any other samples from Augustine volcano.

We have analyzed over 50 MIs from these basaltic clasts, hosted in olivines that range in composition from Fo_{76} to Fo_{86}, although >80% of the inclusions are trapped in $Fo_{80–83}$ olivines (whole-rock samples contain up to Fo_{89} olivine). Within the MI population, we found only two that overlap in composition with the whole-rock hosts (Fig. 6a). These two MIs are anomalous in that they have very high Ca contents (>13·5 wt %) and are hosted in primitive olivines (Fo_{86}). Such compositions are generally interpreted to have resulted from dissolution–precipitation reactions that have occurred in deep mush zones, driving their compositions far from that of the bulk liquid (Schiano *et al.*, 2000; Danyushevsky *et al.*, 2004). The remainder of the MIs plot on the MgO–FeO* array defined by the rest of the volcanic rocks from Augustine, including groundmass from the same samples (Fig. 6a). Thus we support previous inferences that the basaltic whole-rocks have accumulated crystals, and propose that the olivine-hosted MIs from these rocks are better samples of the magmatic liquid.

Water contents measured in the olivine-hosted MIs from Augustine are the highest in the Aleutian arc (>7 wt % H_2O), and at present, are the highest reported in basaltic MIs in the world (Wallace, 2005; Zimmer, 2009). Such water concentrations are consistent with the water concentrations measured in clinopyroxenes from one of the same samples (05AUNY17; Wade *et al.*, 2008), which are in equilibrium with melt containing 3·5–6·5 wt % H_2O. Augustine water contents correlate positively with sulfur

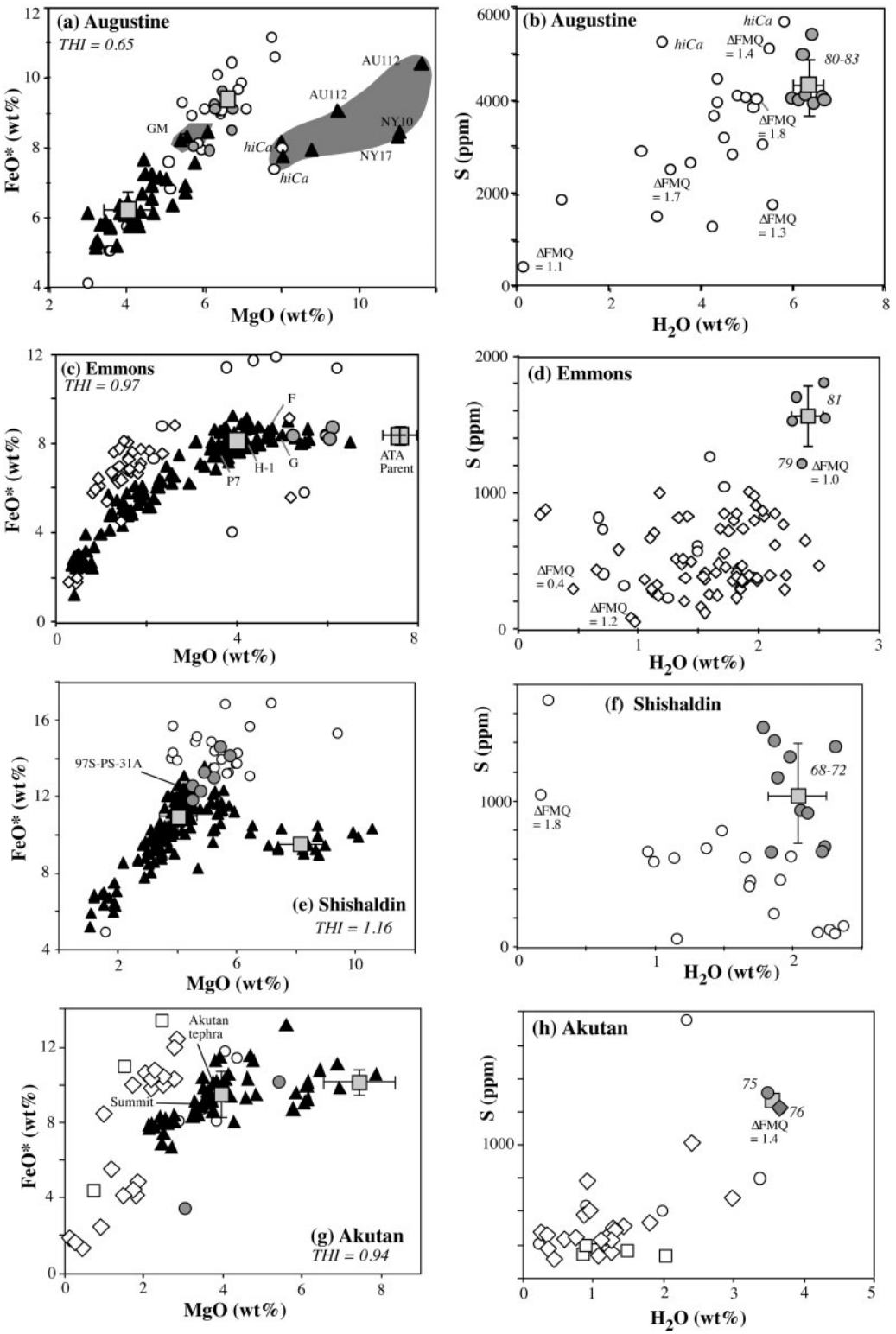

Fig. 6. Whole-rock and melt inclusion data for eight Aleutian volcanoes used to calculate THI and average undegassed H_2O. Left-hand panels show MgO vs FeO* data. Filled triangles are whole-rock data (melt inclusion host samples are labeled); gray symbols are melt inclusions used to calculate THI; open symbols are melt inclusions that are excluded from the THI calculation, because they are either degassed or evolved (see text). Gray squares give $Fe_{4\text{-}0}$ and $Fe_{8\text{-}0}$ (or maximum FeO*) used to calculate THI. Right-hand panels show H_2O and sulfur concentrations in melt inclusions. Circles are olivine-hosted melt inclusions, diamonds are pyroxene-hosted melt inclusions, and squares are plagioclase-hosted melt inclusions. Gray symbols are generally least degassed and are used to calculate average H_2O relevant to the THI. Some melt inclusions labeled with An (anorthite), Mg-number, or Fo (forsterite) content of host crystal, and with fO_2 (labeled as ΔFMQ) as determined from sulfur Kα peak shifts (Table 2). Major element and volatile data for melt inclusions are given in Electronic Appendix E. Data sources for whole-rocks are given in Electronic Appendix A; new major element data for whole-rocks are given in Electronic Appendix D.

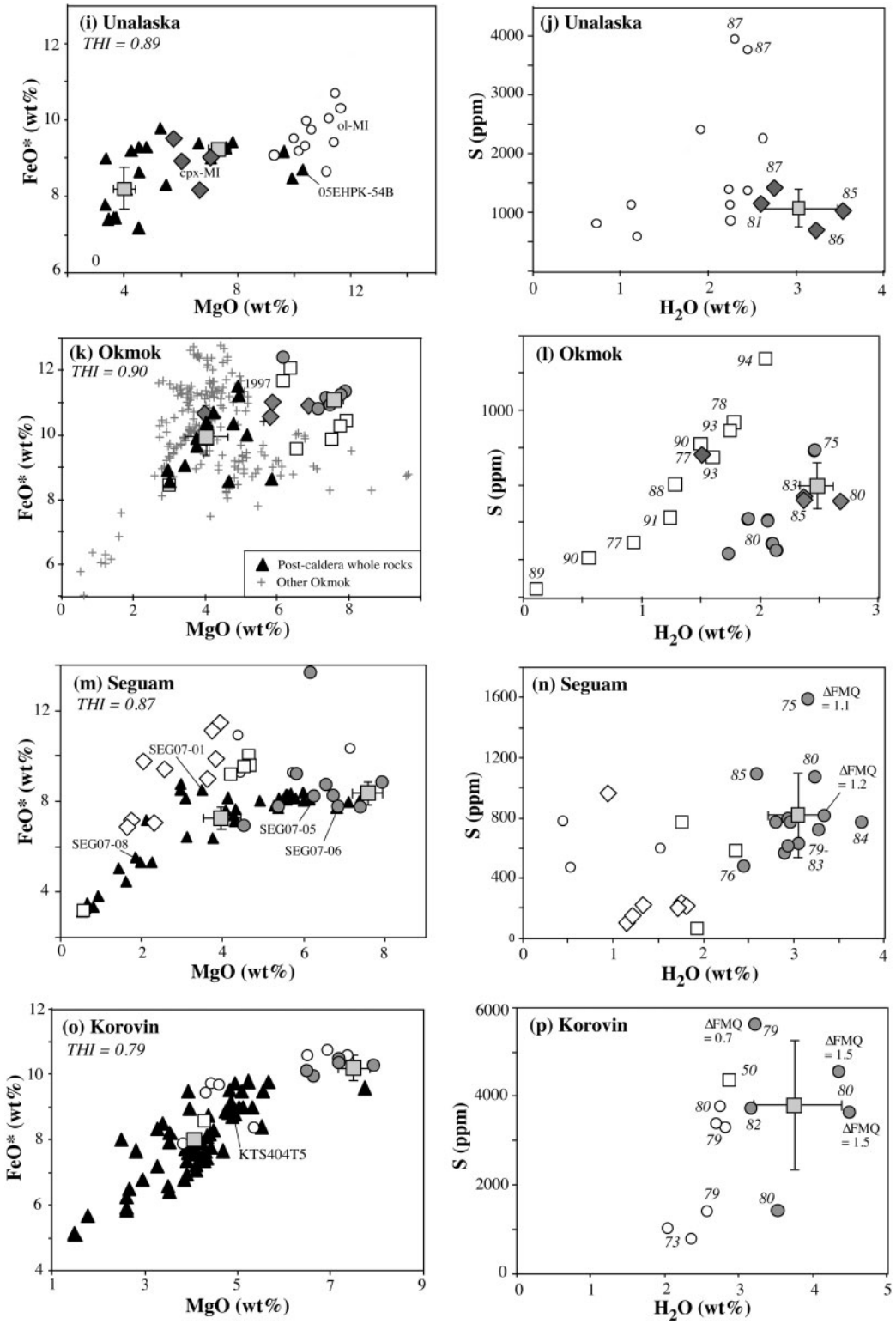

Fig. 6. Continued.

contents (Fig. 6b), which are also among the highest in the world, in excess of 5000 ppm total S. The coupled decrease in H_2O and S is probably driven in part by degassing during magma ascent, and therefore H_2O contents in the primary magma may be even higher than 7 wt %. SKα scans of three MIs indicate that 51–81% of the sulfur is dissolved as SO_4^{2-}, yielding fO_2 of ΔFMQ +1·0 to 1·7 (i.e. 1·0–1·7 log units above the FMQ buffer). Micro-μXANES (X-ray absorption near edge structure) analysis of one MI yields 30% $Fe^{3+}/\Sigma Fe$ (Kelley & Cottrell, 2009), consistent with ΔFMQ +2·1 [using $Fe^{3+}/\Sigma Fe$ and the relationship given by Kress & Carmichael (1991)].

To calculate the THI for Augustine, and to assess the magmatic water contents appropriate to its differentiation, we highlight in Fig. 6b the group of least degassed MIs, with generally >4000 ppm S and averaging ~6·5 wt % H_2O. These inclusions also define a coherent, primitive group in MgO–FeO* space that provide a minimum constraint on $Fe_{8\cdot0}$. Combining this with $Fe_{4\cdot0}$ derived from whole-rock samples yields a THI of 0·65, which is among the lowest in the world. This value is nonetheless dependent on combining Pleistocene mafic melt inclusions (for $Fe_{8\cdot0}$) and modern andesitic eruptive rocks (for $Fe_{4\cdot0}$). Clearly, this is not ideal, as the magmas of Augustine cannot have crystallized along a single liquid line of descent for over 20 000 years, as is evident from significant changes in incompatible element ratios over this time (e.g. Johnson *et al.*, 1996; Zimmer, 2009). Despite this, the modern magmas and Pleistocene melt inclusions form an overlapping linear array in MgO–FeO*, and the THI is not appreciably different if calculated from the MI data alone (but still excluding the degassed, high-Fe MIs and the low-Fe Pleistocene whole-rock accumulates). High water contents and strong Fe depletion are dominant features of Augustine magmas, given the current data available.

Emmons Caldera

Melt inclusions hosted in pyroxene, plagioclase, and rare olivine were selected from scoria lapilli samples described by Anderson (1979), collected from cinder cones P4, P7, G, F, and H within Emmons Caldera. The post-caldera cinder cones are late Pleistocene in age, and the erupted magmas are basaltic andesite to andesite in composition (Fig. 6c).

The MIs encompass a compositional range greater than that of the scoria hosts, from basaltic (rare) to dacitic (common) compositions (Fig. 6c). The basaltic MIs are noteworthy in that they are more primitive than the host scoria, are hosted in the most primitive olivines (Fo_{79-81}), and preserve the least degassed volatile compositions (>1500 ppm S and >2·5 wt % H_2O; Fig. 6d). The vast majority of the MIs, however, are dacitic, degassed (<1000 ppm S, <50 ppm CO_2, and <2 wt % H_2O), and hosted in pyroxenes, plagioclases, and evolved olivines (most with Fo_{70-76}, but some as low as Fo_{61}). SKα scans of three MIs indicate that 14–56% of the sulfur is dissolved as SO_4^{2-}, yielding fO_2 of ΔFMQ +0·36 to 1·24. The large range in fO_2 may be caused by Fe loss from some MIs, which may increase fO_2 and leave sulfide globules in MIs (Danyushevsky *et al.*, 2002), as occasionally observed in Emmons MIs. However, one of the least degassed MIs (H-1oliv3mi2, S >1000 ppm) yielded fO_2 = ΔFMQ +1·0, which is probably representative of the Emmons basaltic parent.

In calculating THI for Emmons, we used the least degassed, basaltic MIs to constrain $Fe_{8\cdot0}$ at ~8·5 wt % FeO*. Although these most primitive compositions have only ~6 wt % MgO, their FeO* contents are similar to those of the most primitive scoria, indicating no change in FeO* from 4 to 6 wt % MgO, and suggesting a THI near unity (Fig. 6c). These same basaltic MIs average 2·5 wt % H_2O (Fig. 6d), and we take this as representative of the LLD showing neither Fe enrichment nor depletion. The basaltic MIs reported here conform in their major element and volatile concentrations to the Emmons parental melt calculated by Anderson (1979) and labeled ATA Parent in Fig. 6c. The more degassed inclusions show both Fe loss (as noted above) and Fe enrichment (as might occur during plagioclase fractionation upon degassing), and most contain <3% MgO and so are outside the range of the THI. Clearly, more primitive samples of the Emmons magmas are desirable, but given the coherence between the least degassed MIs and the scoria whole-rocks, we take them as representative of the dominant magma erupted from these cones within the Emmons caldera.

Shishaldin volcano

Olivine-hosted MIs were picked from Holocene scoria sampled from Shishaldin's summit in 1997 (97S-PS-31). The whole-rock hosts to the MIs are basaltic and have intermediate MgO contents, but among the highest FeO* of Shishaldin eruptive rocks (Fig. 6e). Melt inclusions range in composition from basalt to andesite and are hosted in Fo_{61-72} olivines. Most of the MIs (~60%), however, are hosted in Fo_{70-72} olivine, which is close to that in equilibrium with the whole-rock ($Fo_{69\cdot4}$ in 97S-PS-31A). The FeO* content of most of the MIs is notably higher than any whole-rocks (Fig. 6e), similar to MIs reported from the 1999 eruption (Stelling *et al.*, 2002). The three MIs with the highest FeO* have undergone the greatest amount of post-entrapment crystallization (>12%), and the other high-FeO* MIs are among the most degassed (<2 wt % H_2O). These MIs also have low Al_2O_3 concentrations (<14 wt %, not shown), which, with their high FeO*, probably derive from local plagioclase crystallization driven by the loss of H_2O from the host liquid during decompression. Three of the least degassed MIs, however, overlap in their FeO* with the whole-rocks. Thus, we consider the MI population with the highest H_2O and S

contents as being most representative of the Shishaldin bulk magma. The average of these MIs is ~2 wt % H_2O (Fig. 6f), which is the lowest magmatic water content measured in the Aleutians and among the lowest water content in arc magmas globally. The low magmatic water contents are consistent with inclusion entrapment at depths as shallow as in the volcanic conduit (4 km; Vergniolle & Caplan-Auerbach, 2006). SKα scans of one inclusion indicate that 84% of the sulfur is dissolved as SO_4^{2-}, yielding fO_2 of ΔFMQ +1·8. However, this inclusion has among the highest S but lowest H_2O of the MI population (Fig. 6f), suggesting that it probably underwent H^+ diffusion and consequently a post-entrapment increase in fO_2 (Danyushevsky *et al.*, 2002).

The whole-rocks from Shishaldin define what appears to be a consistent LLD, with little initial change in FeO*, consistent with olivine fractionation, then an increase from ~6 to 4 wt % MgO as plagioclase begins to crystallize. At 4–5 wt % MgO, FeO* decreases sharply as magnetite probably crystallized. This mineralogy is consistent with the plagioclase + olivine phenocrysts observed in the scoria samples. The THI for Shishaldin (1·16) reflects this tholeiitic LLD, with $Fe_{4·0}$ of ~11 wt % being the highest in the Aleutians. Fe peaks at even higher concentrations (~13 wt %) at ~5% MgO, and if this composition were used to calculate the THI, the total Fe enrichment would be 1·4, approaching the low end of MORB (Fig. 4). The parental magma ($Fe_{8·0}$ = 9·5 wt %) is well constrained by an aphyric bomb and low-crystallinity lavas from the Holocene Olivine Cone, all with 8–9 wt % MgO and FeO* ~9·0–9·5 (Fournelle, 1988; Stelling *et al.*, 2002). The high degree of Fe enrichment coupled with low H_2O contents of Shishaldin magmas make this volcano an arc end-member.

Akutan volcano

A dedicated sampling campaign in 2005 focused on mafic ash and lapilli from the modern volcano. Some of the samples that yielded MIs (RKAK-1, 05AKTAP-09a and -14) are correlated with the Akutan Tephra, a scoria deposit up to 2 m thick, that formed during the major eruption that created the present summit caldera (1611 years BP; Waythomas, 1999). Other samples (05AKTAP-12a and -18a) are dark ash layers that post-date the Akutan Tephra. These scoria samples, and in fact most of the historical eruptive rocks, are basaltic andesite in composition (with ~4 wt % MgO). There are no analyzed samples from the modern volcano that have >6 wt % MgO (see references to Table 1). More primitive lavas, with up to 8 wt % MgO, occur on the eastern half of the island, and are Pliocene in age (Richter *et al.*, 1998).

Pyroxene-, plagioclase-, and olivine-hosted MIs encompass a wider range of compositions than the host tephra, from basalt to rhyolite. Olivine hosts (from sample 05AKTAP-18a only) vary in composition from Fo_{67} to Fo_{75}. Taken together, the MIs form a coupled H_2O–S degassing trend (Fig. 6h), with the least degassed MIs hosted in the most primitive olivine and clinopyroxene (Mg-number 75–76). SKα scans of one inclusion indicate 65% of dissolved sulfur as SO_4^{2-}, yielding fO_2 of ΔFMQ +1·4.

The THI for Akutan is based almost entirely on the whole-rock data, as most of the melt inclusions have <3 wt % MgO (Fig. 6g) and fall outside the range used to calculate THI. The least degassed olivine-hosted inclusion has the highest MgO concentration (~5 wt %) of the MI population. $Fe_{4·0}$ is well constrained from abundant whole-rocks from modern Akutan, including the Akutan Tephra (labeled AT in Fig. 6g). The parental composition ($Fe_{8·0}$) relies entirely on Pliocene lavas from the eastern side of the island, which are the only samples from Akutan with >7 wt % MgO. Taken together, the whole-rocks give a THI of 0·94, and the least degassed MIs give H_2O of ~3·7 wt %.

Unalaska island

A dedicated sampling campaign in 2005 focused on mafic tephra from two Quaternary cones on the SW flank of Makushin volcano on Unalaska island, Pakushin and Angela's Cone. Pakushin is a large (>1000 m elevation), composite cone with multiple craters (22 ± 5 ka; McConnell *et al.*, 1998). Melt inclusions were analyzed from the outer 1 cm of a highly vesicular bomb (7 cm) collected from the base of Pakushin cone. Angela's Cone is a nearby, newly discovered cinder cone highly eroded by ice, streams, and weathering, probably of pre-Holocene age. Samples from Angela's Cone consist of abundant olivine and clinopyroxene phenocrysts and small dark clasts in a highly altered, orange matrix. No whole-rock analyses were attempted because of extreme sample alteration. Most of the material that has been erupted from Makushin volcano consists of basaltic andesites and andesites, with the notable exception being volcanic rocks from numerous flank cones, which include primitive basalts. Indeed, the Pakushin bomb we studied has over 10 wt % MgO (Fig. 6i), and we suspect that the mafic clasts from Angela's Cone are as primitive, given their similar melt inclusions and olivine population (see below).

Melt inclusions from Pakushin and Angela's Cone are hosted predominantly in primitive olivine ($Fo_{86–89}$), with some Pakushin melt inclusions also hosted in clinopyroxene (Mg-number 82–87). The olivine-hosted inclusions form a linear trend (Fig. 6i), with FeO* and MgO increasing together and maintaining a ratio required to be in equilibrium with $FO_{87(±1)}$ olivine. This trend is unexpected for magma fractionation and is probably an artifact of the olivine addition calculation, as the MIs with the highest MgO and FeO* are those that are the most out of equilibrium with their host olivine, requiring >15 wt % olivine addition to achieve equilibrium. These compositions are

unlikely to represent magmatic liquid compositions, and point towards a more complex process than sidewall post-entrapment crystallization to form their final composition, and/or significant Fe^{3+}. On the other hand, the olivine-hosted MIs with the lowest MgO (<11 wt %) have compositions similar to the whole-rock and are hosted in Fo_{87} olivines, which would be in equilibrium with the whole-rock liquid (Fig. 6i). We thus conclude that the whole-rock and the lower-MgO olivine-hosted MIs represent reasonable primitive liquid compositions for Makushin. The clinopyroxene-hosted melt inclusions are more evolved, with <8 wt % MgO, but nonetheless overlap with other Makushin whole-rocks. The H_2O content of the MIs extends up to 3·5 wt %, with the highest contents being in the clinopyroxene-hosted MIs from Pakushin (Fig. 6j). Some of the olivine-hosted MIs are very S-rich, with two from Angela's cone having up to 4000 ppm. No SKα data were collected from MIs from Pakushin or Angela's Cone.

In calculating the THI for Makushin, we rely largely on the whole-rock data, as only one MI falls within the range of MgO (3–5 wt % and 7–9 wt %) used to calculate $Fe_{4·0}$ or $Fe_{8·0}$. All of the olivine-hosted MIs (and the Pakushin whole-rock) are too primitive (>9 wt % MgO), and all but one of the clinopyroxene-hosted MIs are too evolved (<7 wt % MgO) for calculating $Fe_{8·0}$. Nonetheless, the $Fe_{8·0}$ calculated from the whole-rocks (9·2 wt %) is consistent with the parental FeO* content (~9 wt %) inferred from the more mafic whole-rocks and the olivine-hosted MIs that required the least olivine addition. Combining this with $Fe_{4·0}$ of 8·2 gives a THI of 0·89. To obtain the average H_2O content (3·0 ± 0·2 wt %), we use clinopyroxene-hosted MIs only, because they are the only ones that overlap in composition with the portion of the liquid line of descent reflected in the THI, between 4 and 8 wt % MgO.

Okmok volcano

Okmok volcano on Umnak island had two major caldera-forming eruptions at ~12 000 years BP and 2050 years BP (Larsen *et al.*, 2007); post-caldera activity has included over 10 eruptions during the last century. The MIs studied here derive from a tephra sample (01NYO-10) erupted in 1997. The moderate Hawaiian to Strombolian 1997 eruption lasted ~2 months, and generated a 10 km ash plume and 6 km long lava flow emanating from Cone A on the caldera floor (Patrick *et al.*, 2003). The 1997 tephra is basaltic to basaltic andesite in composition, similar to other material erupted from the intra-caldera cones (Finney *et al.*, 2008) but has the highest FeO* of any post-caldera magma (Fig. 6k). Melt inclusions were analyzed within olivine, clinopyroxene and plagioclase phenocrysts.

The most striking feature of the 1997 Okmok MI data is the difference between MIs hosted in plagioclase and those hosted in the mafic phenocrysts, olivine and clinopyroxene (Fig. 6l). The plagioclase-hosted MIs form a highly systematic trend in H_2O vs S contents, consistent with degassing upon ascent. The trend, however, is displaced significantly to lower H_2O than that for the MIs hosted in the mafic phenocrysts. Moreover, the plagioclase hosts ($An_{77–94}$) are largely out of equilibrium with both the whole-rock and the MIs, given the water contents measured (<3 wt %) and the partitioning relationships given by Sisson & Grove (1993*a*). Anorthite contents >81 require either higher H_2O contents in the magma than measured here (>2·5 wt %) or growth in magmas with high Ca/Na. Both the lower H_2O found in the plagioclase-hosted melt inclusions and the lack of equilibrium with the major host crystal are consistent with the MIs remaining open to the surrounding matrix liquid during ascent, as has been demonstrated with Mt. St. Helens samples (Blundy & Cashman, 2005). The major element contents of the plagioclase-hosted MIs also diverge widely from those in the other MIs or from other whole-rocks, and so are not used to define either the H_2O content or THI for 1997 Okmok. The mafic phenocrysts host MIs that record uniformly higher H_2O contents (mostly >2 wt % H_2O), and have more systematic and overlapping major element compositions. These MIs also generally have higher MgO than the whole-rock, consistent with the high Mg-number of their olivine hosts (80–85), which are not in equilibrium with the whole-rock (~Mg-number 72). Thus, we interpret the MIs hosted in the mafic phenocrysts as being representative of the mafic parents to the 1997 magma.

In calculating THI, it is important to recognize that Okmok has erupted a wide variety of magmas, as might be expected over its history of caldera-forming eruptions that have altered the plumbing system and volume of the volcano. Examination of all published Okmok whole-rock data reveals an enormous range in FeO* at any given MgO, including among the most Fe-rich compositions in the Aleutians (>12 wt % FeO*). For this reason, we restrict our analysis to the post-caldera magma output (Finney *et al.*, 2008), which is more restricted compositionally (Fig. 6k), and most relevant to the 1997 melt inclusions examined here. Nonetheless, even the post-caldera magmas poorly define any LLD, and so calculation of the THI is not straightforward for Okmok. In practice, $Fe_{8·0}$ derives from the five olivine-hosted MIs with 7–8 wt % MgO, whereas $Fe_{4·0}$ derives from the post-caldera whole-rocks with 3–5 wt % MgO, which appear to define an Fe-decreasing LLD. Together, the MIs and whole-rocks yield a THI of 0·90 for post-caldera Okmok. We take the initial H_2O content of the magma to be ~2·5 wt %, the average of the four MIs with the highest H_2O (Fig. 6l).

Seguam volcano

A dedicated sampling campaign in 2007 studied the Holocene tephra section erupted from Pyre Peak, the

western and more recently active of two volcanic centers on Seguam island. Seguam has a 318 kyr eruptive history, where the past 9 kyr have seen both the sector-collapse of Wilcox volcano in the east and caldera formation in the west, followed by the eruption of Pyre Peak lavas and tephras as recently as 1992–1993 (Jicha & Singer, 2006). Everything from rhyolite to basalt has erupted from the post-collapse Holocene vents (Jicha & Singer, 2006). Prior to 9 ka, magmas evolved along a simple ^{230}Th ingrowth curve for ~100 kyr, consistent with a single, deep magma reservoir (Jicha *et al.*, 2005). A shift in the Th and Sr isotopic composition of the magmas at 9 ka reflects an influx of new parental magma into the reservoir, coincident with the cone collapse eruptions. For this reason, and because our volatile measurements are made on the youngest tephra, we focus here on the Holocene (≤ 9 ka) volcanic products of Seguam only.

Melt inclusions were found in olivine, plagioclase and clinopyroxene from ash and lapilli tephra samples that range in composition from basalt to dacite. The least degassed, most mafic MIs were found in olivines ($Fo_{80–85}$) from basaltic tephra of the 1977 eruption of Pyre Peak (SEG07-05 and SEG07-06; Fig. 6n). The MIs from the other, more evolved samples (SEG07-01, -07, -08, and -10) were hosted in plagioclase or clinopyroxene and appear to be degassed based on their lower H_2O (<2·5 wt %) and S (<600 ppm) contents (Fig. 6n). These MIs generally have higher FeO* and lower Al_2O_3 than the MIs with higher H_2O content or any whole-rock, consistent with enhanced plagioclase fractionation driven by loss of H_2O from the melt.

In assessing the THI of Seguam, the Holocene volcanic rocks define what appears to be a coherent liquid line of descent from 8 to 1 wt % MgO (Fig. 6m). The MIs with the highest H_2O contents (>2·5 wt %) conform well to the whole-rock trend. The combined LLD shows roughly constant FeO* at high MgO (>5 wt %), consistent with olivine-dominant fractionation, then decreasing FeO* below 4 wt % MgO, consistent with magnetite fractionation. The THI is thus moderately calc-alkaline, with a value of 0·87. The H_2O concentrations in the mafic MIs range up to 3·7 wt %, but we take the average of the MIs that correspond to the whole-rock THI to be 3·0 ± 0·3 wt % H_2O.

Korovin

Atka island contains several volcanic centers, including Korovin volcano, which has been active historically and is the source of the tephra and melt inclusions studied here. Sample KTS404T5 is mafic lapilli from a tephra section several kilometers from the Korovin summit. It is basaltic andesite in composition, like most of the erupted material from Korovin.

Olivine ($Fo_{73–82}$) and plagioclase (An_{50}) host basaltic and basaltic andesite MIs that overlap with Korovin whole-rock compositions and are commonly more mafic than the whole-rocks (Fig. 6o). The most mafic MIs are trapped in the most forsteritic olivines and have the highest H_2O contents, ranging up to 4·5 wt %. Sulfur contents in many of the melt inclusions are very high (4000–5500 ppm). H_2O and S generally decrease together with Fo content (Fig. 6p), consistent with the simultaneous degassing of both species during crystallization.

The THI for Korovin requires using the MI data to calculate $Fe_{8·0}$, as there are few samples with MgO contents >6 wt %. The most hydrous mafic melt inclusions, trapped in the most forsteritic olivine, give a well-defined $Fe_{8·0}$ of 10·2 ± 0·2. This is consistent with, but somewhat higher than, the highest FeO* measured in Korovin–Atka whole-rocks (9·6–9·8 wt %). $Fe_{4·0}$ is well constrained from abundant Korovin whole-rocks in this range, giving a value of 8·0 ± 0·1, for a final THI of 0·79. The MIs used to constrain parental Korovin $Fe_{8·0}$ have an average H_2O content of 3·7 ± 0·3 wt %. Thus Korovin magmas are slightly more calc-alkaline, and slightly wetter, than those of nearby Seguam.

Summary: H_2O and THI in the Aleutians

The above discussion of melt inclusion and whole-rock data allows us to compare least degassed H_2O and THI in eight Aleutian volcanoes (Fig. 7a). Based on the THI variations, Aleutians volcanoes range from tholeiitic (Shishaldin, with THI = 1·16) to strongly calc-alkaline (Augustine, with THI = 0·65). This variation does not correlate simply with location along the arc, nor variations in subduction parameters, and its underlying cause in the Aleutian volcanic arc is the subject of a separate study. Nonetheless, these distinctions, based on the THI, generally conform to those derived from the classic MgO/FeO*–SiO_2 diagram (see symbol shading in Fig. 7a and Table 3), where Augustine and Seguam plot fully in the CA field, Shishaldin, Akutan, and Okmok are TH, and others (Emmons, Unalaska, and Korovin) straddle the CA-TH dividing line (e.g. transitional TH or CA; Kay & Kay, 1994). The THI further distinguishes those transitional volcanoes such as Korovin (THI <0·9) from Emmons and Unalaska (THI >0·9). A comparison with other classification schemes is listed in Table 3, including the THI, CA/TH Index (related to the ratio of slopes on the SiO_2 vs FeO*/MgO diagram; Hora *et al.* 2009), and high-, medium-, and low-Fe suites (based on finer divisions on the SiO_2 vs FeO*/MgO diagram; Arculus, 2003). The THI and the CA/TH Index vary inversely, as is expected, and the 'high-Fe' volcanoes have higher THI (≥0·9) than the 'low-Fe' volcanoes (≤0·9). These systematics indicate that Miyashiro's dividing line between CA and TH lies at a THI of ~0·9 for the Aleutians, and not at 1·0 as required by true Fe enrichment.

The THI not only quantifies finer variations in Fe enrichment, but also strongly anti-correlates with H_2O

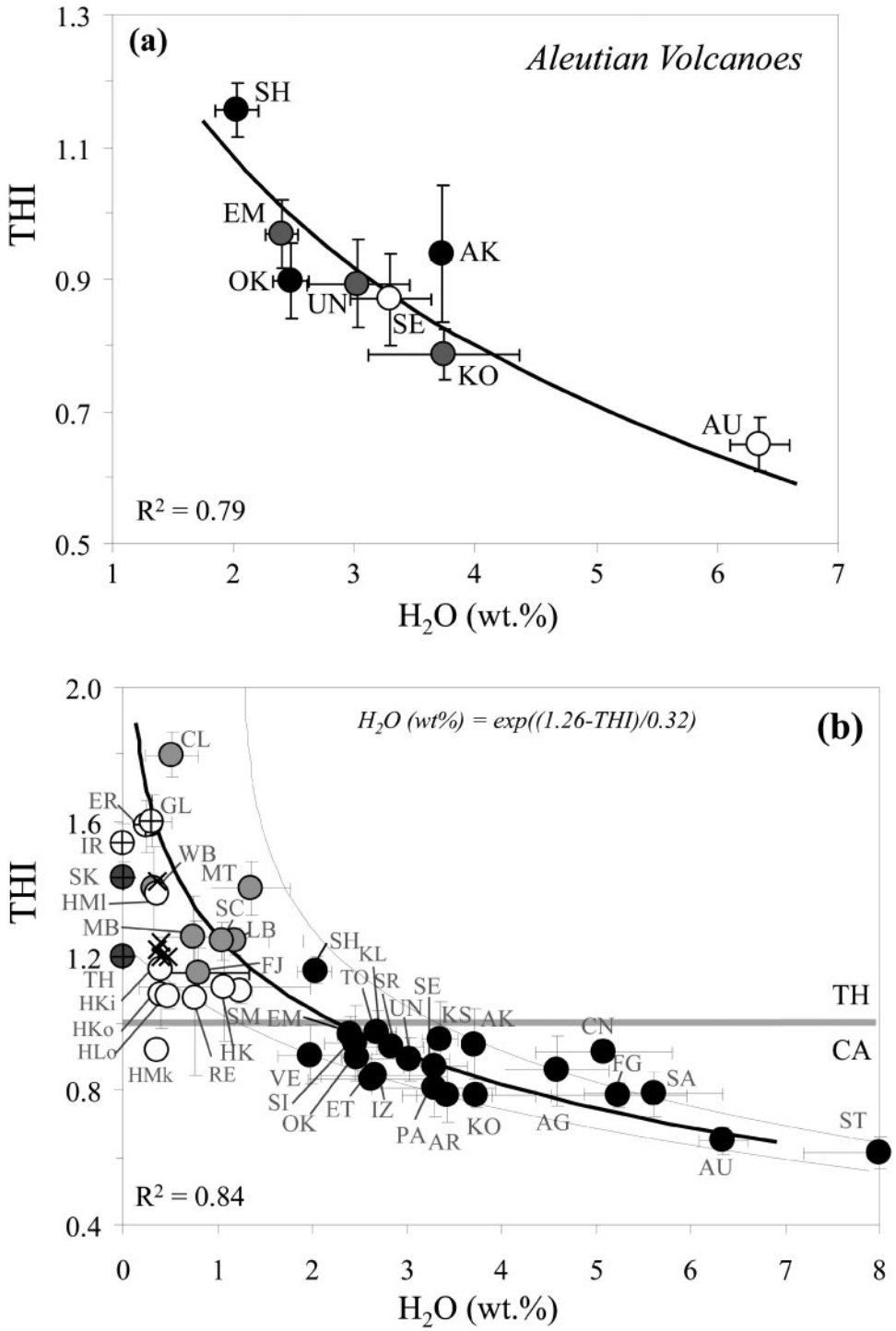

Fig. 7. THI vs H_2O. (a) THI and average maximum magmatic water content measured in melt inclusions (as in Fig. 6) for eight volcanoes from the Aleutian volcanic arc (Table 1). Abbreviations as in Fig. 5. Filled circles are TH, open circles are CA, and gray circles are transitional, based on the SiO_2 vs FeO*/MgO diagram of Miyashiro (1974). (b) THI vs H_2O for arcs (filled circles), back-arc basins (gray circles), ocean islands (open circles), and mid-ocean ridges (open circles with crosses). THI for two layered mafic intrusions (gray circles with crosses) shown at 0 wt % H_2O (no measured H_2O). THI for Hawaii is also shown as calculated at maximum FeO* (×; see text for details). Regions lacking water data (plotted at 0% H_2O) and ocean islands are not included in regression. THI error bars (2σ standard error) are propagated from standard deviation of the mean $Fe_{4\text{-}0}$ and $Fe_{8\text{-}0}$, and H_2O error bars are 1σ standard deviation (see Table 1 for values and abbreviations). Best-fit curve (logarithmic) to data determined by reduced major axis regression. The 95% confidence interval on H_2O (dashed lines, read horizontally off the *x*-axis) gives a roughly similar error (~±1·2 wt %) at both high and low water contents. Data sources and a description of THI and H_2O calculations for volcanoes outside the Aleutians are given in Electronic Appendix A.

Table 3: Comparison of CA-, TH-based classification for Aleutian magmas (see text for details of classification systems)

Volcano	THI	CA/TH Index[1]	Fe (Arculus)[2]	Miyashiro[3]
Augustine	0·65	1·73	loFe	CA
Emmons	0·97	0·89	meFe	transitional[4]
Shishaldin	1·16	0·4–1	hiFe	TH
Akutan	0·94	0·71	hiFe–meFe	TH
Unalaska	0·89	0·81–1·47	meFe	transitional
Okmok	0·9	0·69	hiFe	TH
Seguam	0·87	1·06	loFe	CA
Korovin	0·79	0·97	meFe	transitional

[1]Hora *et al.* (2009).
[2]Arculus (2003).
[3]Miyashiro (1974).
[4]Transitional magmas straddle the CA–TH dividing line proposed by Miyashiro (1974); after Kay & Kay (1994).

($R^2 = 0{\cdot}79$; Fig. 7a). The co-variation between H_2O and THI is stronger than for other measures of calc-alkalinity based on the SiO_2 vs FeO*/MgO diagram. Such a correlation between THI and H_2O in the Aleutian volcanic data points to H_2O as a primary control on Fe depletion and generation of the CA trend. Next we test this prediction by examining magmatic suites from other subduction zones and tectonic settings.

H_2O and THI in global magmatic studies

Average H_2O contents and THI for 41 magmatic suites from different tectonic settings are plotted in Fig. 7b (Table 1). Data references (in addition to the GEOROC and PetDB databases) and a brief description of how THI and H_2O were calculated for each volcanic suite are found in Electronic Appendix A. Examples include arc volcanoes (Aleutians, Central America, Cascadia, Ryukyu, Mariana, Aeolian Islands, and the alkaline volcanoes Etna and Vesuvius), as well as mid-ocean ridges, back-arc basins, and ocean island volcanoes. Despite significant variations in subduction parameters for different arcs (e.g. age of subducting crust, slab dip, thermal regime, subducting sediment composition; Plank & Langmuir, 1998; Syracuse & Abers, 2006), and variations in the melting and crystallization processes within different tectonic settings, a strong negative correlation between H_2O and THI persists in the global dataset ($R^2 = 0{\cdot}84$ for logarithmic regression):

$$H_2O\ (\mathrm{wt}\%) = \exp[(1 \cdot 26 - \mathrm{THI})/0 \cdot 32]. \qquad (2)$$

Even though the error envelope expands at low H_2O contents, the uncertainty on H_2O is roughly the same ($\pm 1{\cdot}2$ wt % H_2O) as at high H_2O contents (Fig. 7b).

Arc magmas show the greatest range in THI and H_2O, yet magmas from different tectonic settings occupy distinct regions in Fig. 7b. Back-arc basin magmas have water contents lower than the low end of the range for arc magmas (1–2 wt % H_2O), and THI is correspondingly higher (THI = 1·15–1·80). OIB data overlap with back-arc basin H_2O, but have a large range in THI. These data are excluded from equation (2) and the regression in Fig. 7b for reasons that are discussed below. Only two MOR suites (Galapagos Ridge and East Pacific Rise) have both measured water contents and volcanic rocks that are evolved enough to calculate the THI (e.g. 3–5 wt % MgO), so an additional suite (SE Indian Ridge) is plotted at 0 wt % H_2O (no measured H_2O, and not included in the regression) to illustrate the high THI of MORB suites. Despite the paucity of both kinds of data, MOR magmas clearly have the lowest magmatic water contents (<0·5 wt % H_2O; Dixon *et al.*, 1988; Michael, 1988), and the uniformly highest THI (>1·4), of the magma types plotted in Fig. 7b (see also Fig. 4). Thus, the distinctions observed earlier in THI with tectonic setting (Fig. 4) also pertain to H_2O content. An effective break is observed at around 2 wt % H_2O, above which magmas typically evolve along CA trends, and below which they evolve along TH trends.

DISCUSSION

The strong anti-correlation between THI and H_2O both in the Aleutian volcanic arc and in magmatic suites in general suggests a strong control of water on the development of calc-alkaline differentiation trends. Such a control is expected based on laboratory experiments (see below), which show how water affects the abundance and appearance particularly of plagioclase, but also magnetite and amphibole, on a magma's cotectic. Here we first test whether the THI–H_2O relationship can be quantitatively reproduced from the effects of varying magmatic H_2O contents alone, using laboratory experiments and crystallization models derived from them. We then explore other effects that may go in tandem with H_2O (pressure of crystallization and oxygen fugacity). Finally, we briefly discuss other controls on CA vs TH differentiation in magmatic suites.

The control of water in generating the CA trend

Subduction zone magmas contain greater amounts of dissolved water than mid-ocean ridge, ocean island, or back-arc basin magmas (Fig. 7b), and thus water is an obvious culprit in affecting the way magmatic suites evolve. Existing data show a clear distinction between TH and CA magma differentiation occurring at ~2 wt % H_2O (Fig. 7b). As discussed above, water has three primary effects on the crystallization of magmas: (1) it suppresses the crystallization of plagioclase relative to mafic phases; (2)

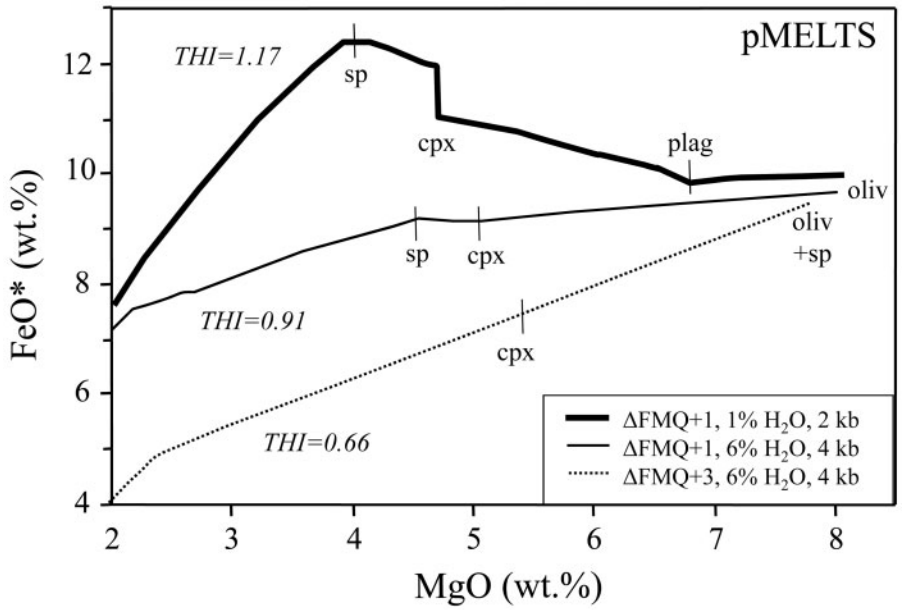

Fig. 8. FeO* vs MgO plot of pMELTS (Ghiorso *et al.*, 2002) results illustrating the effects of magmatic water on the THI. Increasing magmatic water from 1 to 6 wt % decreases the THI as a result of plagioclase suppression. Spinel (magnetite) should also arrive earlier, near the liquidus, with 6 wt % H_2O and ~ΔFMQ +1 (Sisson & Grove, 1993*a*). To simulate this effect, fO_2 is raised to ΔFMQ +3 in pMELTS to force earlier saturation in spinel. With both plagioclase suppression and spinel enhancement, THI approaches strongly CA values (<0·7) as observed in the wettest arc magmas (Fig. 7b). Starting composition is ID18 from Okmok volcano (Nye & Reid, 1986).

it suppresses the crystallization of all silicates relative to spinel; (3) it stabilizes amphibole. All of these effects lead to Fe depletion during crystallization. The suppression of plagioclase crystallization allows Fe-bearing minerals such as olivine and clinopyroxene to deplete the magma in Fe (Yoder, 1954). Subsequent experimental work has documented the suppression of all silicate minerals, with plagioclase suppressed to the greatest extent, relative to Fe–Ti oxides (Baker & Eggler, 1987; Sisson & Grove, 1993*a*; Asimow & Langmuir, 2003; Grove *et al.*, 2003; Berndt *et al.*, 2005). At high H_2O contents, a spinel phase may appear with olivine on the liquidus of hydrous basalt (Sisson & Grove, 1993*a*), causing a dramatic reduction of Fe early in the liquid line of descent. Amphibole may also be stabilized in magmas with >~4 wt % H_2O (Sisson & Grove, 1993*a*; Moore & Carmichael, 1998) and moderate Na_2O, and its relatively high Fe content may also drive Fe depletion, particularly in more evolved melts. Thus, there is a strong petrological response to adding water to mafic magma that favors low THI, CA differentiation trends. Here we address whether the predicted effects are large enough to generate the magnitude of the relationship between THI and H_2O observed in existing data (Fig. 7b).

To explore the effects of water on magmatic liquid lines of descent, we first make use of pMELTS, a model for quantifying the effects of melting and crystallization based on the thermodynamic properties of silicate melts (Ghiorso & Sack, 1995; Ghiorso *et al.*, 2002). Although pMELTS was developed to improve mantle melting calculations, it includes a larger experimental database of hydrous melt compositions and a more recent equation of state for water than MELTS (Ghiorso *et al.*, 2002), and we have found it more accurate than MELTS in predicting phase equilibria for hydrous magmas in the crust (Wade *et al.*, 2006). Nonetheless, pMELTS still over-suppresses plagioclase and under-enhances spinel in hydrous systems relative to the experiments of Sisson & Grove (1993*a*, 1993*b*); it also over-stabilizes clinopyroxene (Villiger *et al.*, 2004). These issues prevent the use of pMELTS as an accurate quantitative tool; it is useful, however, in illustrating trends in magma differentiation and how they change as a function of the water content of the melt.

Figure 8 shows a series of liquid lines of descent generated with pMELTS for a basaltic parental melt with different H_2O contents. A relatively dry magma (1 wt % H_2O) crystallizes olivine, plagioclase, clinopyroxene and spinel, in that order, at ΔFMQ +1. When plagioclase appears on the cotectic, there is a dramatic increase in FeO* in the liquid that continues until spinel (magnetite) crystallizes, generating a TH trend with THI of ~1·15. Such a crystallization sequence is typical of relatively dry magmas, such as back-arc basin volcanic rocks, or the driest arc magmas such as those of Shishaldin. A THI of 1·15 at 1 wt % H_2O is very close to that given by the regression of the global data [e.g. equation (2)]. With further addition of H_2O, the main effect is to suppress plagioclase. Increasing H_2O

to 6 wt % generates a liquid line of descent dominated by olivine and clinopyroxene crystallization, with a modest Fe-depletion trend (THI = 0·91). pMELTS probably over-suppresses plagioclase (specifically the albite component) compared with the compilations of Sisson & Grove (1993*a*) and Berndt *et al.* (2005), and in fact pMELTS predicts that plagioclase never crystallizes above 3% MgO when H_2O is >4 wt %. Still, plagioclase suppression can drive fractionation trends from strongly TH (as in dry MORB, where plagioclase crystallizes very early) to modestly CA (as for arc magmas with <3 wt % H_2O).

To generate more strongly CA trends (i.e. THI <0·9), magnetite must crystallize earlier in the LLD, which is an effect that is not reproduced by pMELTS even with 6 wt % H_2O (Fig. 8), despite strong experimental evidence for this. Water depolymerizes silicate melts, with more complex silicates depolymerized to a greater extent, which ultimately favors the crystallization of oxides. For example, Sisson & Grove (1993*a*) used various experimental data to illustrate that a spinel phase may appear on the liquidus of a basalt with 3·5–6·0 wt % H_2O [at ~NNO (nickel–nickel oxide)]. If we force pMELTS to put spinel on the liquidus by raising fO_2 to ΔFMQ +3, then a strong Fe depletion trend ensues. The combined suppression of plagioclase and relative enhancement of spinel generates a THI of ~0·65, much like the wettest arc basalts (e.g. those of Augustine and Shasta). Thus, the full range in THI observed in arc magmas can be explained by 1–6 wt % H_2O, using pMELTS as a tool to generate the plagioclase suppression and spinel enhancement consistent with the experimental study of Sisson & Grove (1993*a*). The simplest explanation for the THI–H_2O arc trend is the opposing effects on Fe of plagioclase suppression and spinel crystallization owing to addition of water to melts.

Water may also stabilize amphibole in the crystallizing assemblage. pMELTS did not predict amphibole saturation above 3% MgO, even for high-Na, wet compositions (>6 wt % H_2O, Na_2O), although this may in part reflect modeled liquids near or above the upper temperature limit for amphibole stability. Amphibole is a common mineral in more silicic magmas (andesites and dacites), although it occurs early in some mafic systems as well (Shasta, Grove *et al.*, 2003; Augustine, Zimmer, 2009; Mascota basaltic andesite, Moore & Carmichael, 1998). Kay & Kay (1985) noted that amphibole was not present in Aleutian tholeiitic magmas (using the Miyashiro diagram) and thus implicated it in the evolution of CA magmas. In many of the calc-alkaline volcanic systems in Fig. 7b, however, amphibole is notably absent (e.g. Seguam, Singer *et al.*, 1992; Cerro Negro, Walker & Carr, 1986; and all the Marianas volcanoes except for Sarigan, where it is a late phase, Meijer & Reagan, 1981); thus, on its own, amphibole may not drive significant variation in THI. Even where present early (e.g. Augustine), the FeO*–MgO content of the amphibole (11–12 wt % FeO* and 14–15 wt % MgO; Zimmer, 2009) is such that it has low leverage on the extent of Fe depletion on the liquid line of descent from 8 to 4% MgO. Thus, amphibole is more common and has a larger effect on Fe depletion later in the crystallization sequence of most arc magmas, whereas plagioclase and spinel have the dominant effect on the early part of the sequence that governs THI variations.

Water and the pressure of crystallization

Magmas can dissolve large quantities of H_2O only at high pressure; thus pressure and water may work together to create low THI in arc magmas. For example, the solubility model of Newman & Lowenstern (2002) predicts that a basaltic liquid at 1100°C with 7 wt % H_2O reaches pure H_2O vapor saturation at ~4 kbar (~15 km), whereas one with 2 wt % H_2O is saturated at 0·4 kbar (~1·5 km). Consequently, moderate crustal pressures are required to maintain high magmatic water contents, and pressure may control H_2O if magmas are saturated with an H_2O-rich vapor within the crust. The issue to resolve is the extent to which the pressure of crystallization may affect the THI independently of water. Crystallization at low pressure must occur at low H_2O concentrations, so in this case there is no independent effect; THI is high at these conditions as a result of early plagioclase and late magnetite crystallization. Crystallization at high pressures (>10 kbar) may become important if arc magmas stall and crystallize at the base of the crust (Annen *et al.*, 2006; Kavanagh *et al.*, 2006), which ranges from <20 km to >60 km for arcs globally (Plank & Langmuir, 1988). At these pressures, the liquidus volumes of clinopyroxene and orthopyroxene expand at the expense of olivine and plagioclase (Grove & Baker, 1984; Sisson & Grove, 1993*a*), and plagioclase may be completely suppressed even in dry magmas (Baker & Eggler, 1987; Gust & Perfit, 1987; Kinzler & Grove, 1992). Garnet also becomes a fractionating phase, as is observed experimentally (Müntener *et al.*, 2001) and inferred from some magma systems. pMELTs confirms the effects of plagioclase suppression and garnet crystallization, but also the early crystallization of high Mg-number clinopyroxene, which actually increases the THI. The net effect of high-pressure crystallization on the THI is thus modest (e.g. a 20% increase in the THI when crystallizing at 10 kbar vs 2 kbar), and at most may lead to some scatter on the THI–H_2O array. We conclude that H_2O and not pressure is the primary driver of THI variations. The main effect of pressure may indeed be to impose the H_2O content of liquids at the level of saturation, but H_2O then affects the phase equilibria in the ways necessary to drive THI to lower values.

Water and oxygen fugacity

Increasing magmatic fO_2 increases Fe^{3+}/Fe^{2+} of the melt, promoting earlier crystallization of spinel (magnetite) and decreasing the THI. Several studies have pointed to water specifically as an oxidizing agent in the sub-arc mantle wedge (e.g. Canil *et al.*, 1994; Brandon & Draper, 1996; Parkinson & Arculus, 1999; Kelley & Cottrell, 2009). In this view, H_2O and fO_2 would be coupled and together would generate the THI variations observed. The extent to which arc magmas are oxidized in their source, however, is controversial. Work by Lee *et al.* (2005) used V/Sc systematics in primitive arc magmas to conclude that their mantle source may be no more oxidized than that of MORB (approximately ΔFMQ −1 to 0). On the other hand, studies based on the fO_2 of mantle xenoliths indicate oxidized mantle in some arc regions (Brandon & Draper, 1996; Blatter & Carmichael, 1998; Parkinson & Arculus, 1999). Although there is disagreement on the oxidation state of the sub-arc mantle, there is broad agreement that arc magmas themselves are oxidized, based on high whole-rock Fe^{3+}/Fe^{2+} (Carmichael, 1991; Lange *et al.*, 1993), the observed dissolved S concentrations that are strongly controlled by fO_2, and the shift of the SKα peak in glasses toward the oxidized species S^{6+} (Carroll & Rutherford, 1988; Wallace & Carmichael, 1994; Rowe *et al.*, 2009). Recent μXANES analyses indicate higher $Fe^{3+}/\Sigma Fe$ and $S^{6+}/\Sigma S$ in arc melt inclusions vs MORB glasses (Jugo *et al.*, 2005; Kelley & Cottrell, 2009; Métrich *et al.*, 2009). The controversy, then, is the extent to which the high fO_2 is generated in the mantle from slab fluids rather than being generated in the crust by magma degassing and crystal fractionation (Mathez, 1984; Carmichael & Ghiorso, 1986). Regardless, arc magmas evolve at more oxidizing conditions than MORB, and this may contribute to CA differentiation.

There are some constraints on the fO_2 of the magmas used to calculate the THI (Fig. 9a). The oxygen fugacity of Aleutian melt inclusions, determined here from sulfur speciation, ranges from ΔFMQ +0·36 to +2·1 (Table 2), although measurements of melt inclusions with the highest H_2O from each volcano (i.e. those that have lost the least amount of water through degassing or diffusion, both of which may affect magmatic fO_2; Mathez, 1984; Danyushevsky *et al.*, 2002; Hauri, 2002; Rowe *et al.*, 2006) define a more restricted range of ΔFMQ +1 to +2·0, which increases somewhat as THI decreases and H_2O increases. This range is comparable with that found in least degassed melt inclusions from other arc volcanoes, both from SKα shifts (Irazú, Benjamin *et al.*, 2007; Arenal, Wade *et al.*, 2006) and μXANES measurements of $Fe^{3+}/\Sigma Fe$ (Sarigan, Kelley & Cottrell, 2009), although some record lower fO_2 ∼ΔFMQ +0·5 (Parícutin, Kelley & Cottrell, 2009; Stromboli, Métrich *et al.*, 2002; Cerro Negro, Sutton *et al.*, 2005). The fact that the inferred fO_2 range in arc magmas (ΔFMQ +0·5 to 2·0) is similar to that calculated from arc peridotite spinels (ΔFMQ +0·3 to 2·0; Parkinson & Arculus, 1999) is consistent with an oxidized mantle source.

This range in fO_2 in arc magmas (∼ΔFMQ +0·5 to 2·0) generally exceeds that found in back-arc basin glasses (ΔFMQ −0·7 to +0·2; Nilsson Farley, 1994; Wallace & Carmichael, 1994) and MORB glasses (ΔFMQ −2 to 0; Christie *et al.*, 1986; Bézos & Humler, 2005; Kelley & Cottrell, 2009). Although there is some disagreement as to the $Fe^{3+}/\Sigma Fe$ in MORB glasses (e.g. Christie *et al.*, 1986; Bézos & Humler, 2005; Kelley & Cottrell, 2009), in the dataset as a whole there is a clear increase in both H_2O and fO_2 from MORB to back-arc basin to arc magmas (Fig. 9a), as has also been demonstrated recently within a single study (Kelley & Cottrell, 2009). Thus, at the scale of the variations between magmas from different tectonic settings, there is strong evidence that H_2O and fO_2 increase together.

Given the co-variation of H_2O and fO_2 and their similar effect on the early appearance of spinel along the LLD, it is somewhat challenging to quantify their individual effects on the THI. A recent experimental study of Berndt *et al.* (2005), however, explored variations in H_2O along two fO_2 buffers on the liquid line of descent of MORB (FMQ and $MnO–Mn_3O_4$, which is ∼ΔFMQ +4). The calculated THI and average H_2O for their experimental liquids (with 4–8 wt % MgO) are superimposed on the global data array in Fig. 9b. At FMQ (and presumably at <FMQ as well), magnetite does not crystallize in liquids with MgO >4 wt % and therefore has no effect on the THI. Thus the main effect at FMQ is the suppression of plagioclase crystallization owing to H_2O, which can generate a range in THI from 1·8 (as in MORB, like the Galapagos; Juster *et al.*, 1989) to THI near unity at almost 5% H_2O (Fig. 9b). Such a THI–H_2O curve for FMQ intersects MORB, but lies well above the back-arc or arc fields. Yet at ∼ΔFMQ +4, spinel crystallizes earlier independent of H_2O, and generates a curve at lower THI for a given H_2O content. With 5% H_2O and ΔFMQ +4, THI is as low as 0·7 in the Berndt *et al.* (2005) experiments, creating a trend that skirts the bottom of the arc field (Fig. 9b). Although ΔFMQ +4 greatly exceeds that measured in the arc data in Fig. 9a, Sisson & Grove (1993*a*) showed that spinel could appear on the liquidus at 5–6 wt % H_2O and NNO (ΔFMQ ∼ +0·7), so results may be similar at more relevant fO_2. Taken together, MORBs have THI consistent with low H_2O and low fO_2 of ≤FMQ, as measured, whereas back-arc and arc THI require more oxidized conditions, between ΔFMQ of 0 and +4, also consistent with measurements. Thus existing data support coupled increases in H_2O and fO_2 to generate the curvature of the global array, as well as fO_2 >FMQ to generate strongly calc-alkaline trends with THI <1.

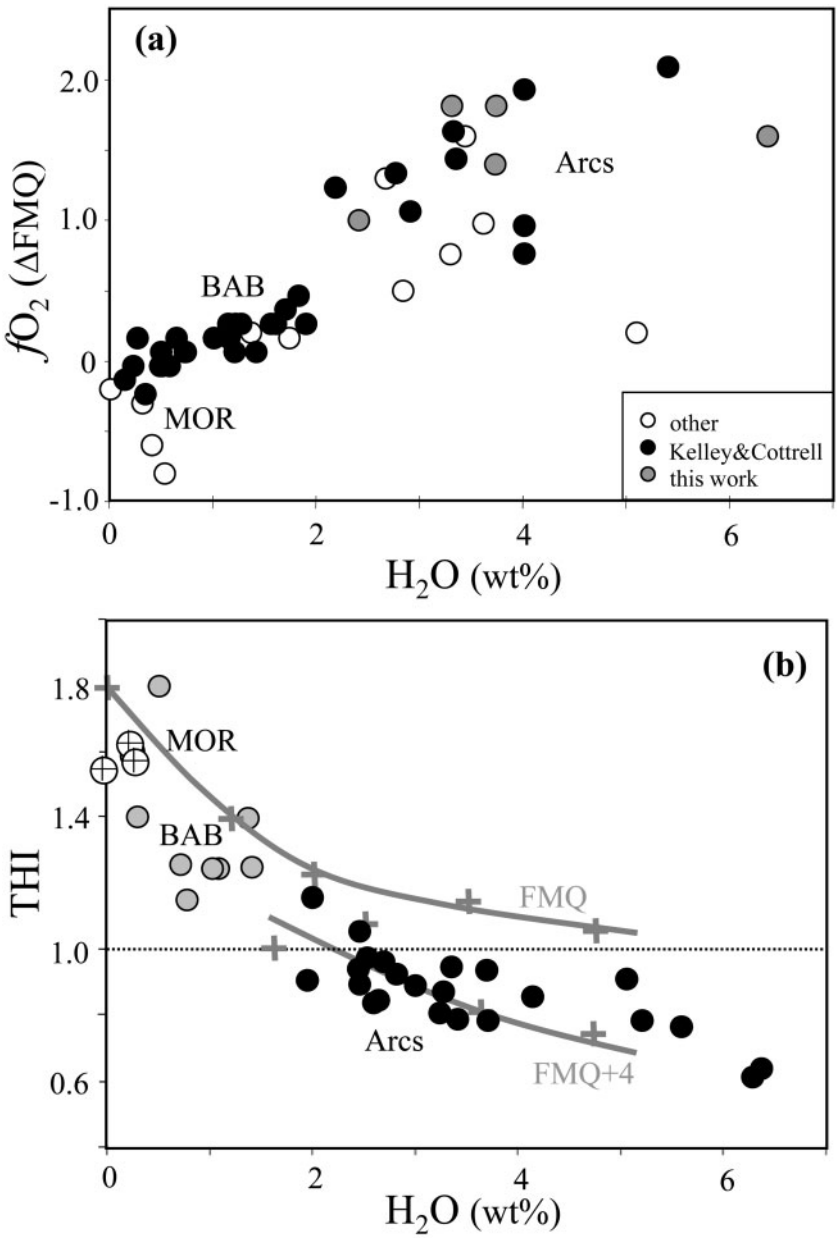

Fig. 9. (a) Estimates of fO_2 vs H_2O in different magmas. Most data are from Kelley & Cottrell (2009) and this study (see Table 2 for data summary and Electronic Appendix G for a more detailed list of data, techniques, and references). (b) Interplay of H_2O and fO_2 on the THI. Data points as in Fig. 7b (excluding OIB and degassed Shishaldin). Grey plus signs and thick lines were calculated from the experimental study of Berndt *et al.* (2005) for MORB composition (Bl) equilibrated along two fO_2 buffers. The data point at FMQ and 0 wt % H_2O is estimated from Galapagos data of Juster *et al.* (1989).

Still, it is noteworthy that almost the entire arc variation ($1{\cdot}1 > \mathrm{THI} > 0{\cdot}7$) can be generated by water variations along a single fO_2 buffer (albeit at ~ΔFMQ +4). If this is also true at intermediate fO_2 (i.e. ΔFMQ of 0 to +4), then arc THI would be predominantly controlled by H_2O variations, with fO_2 generating second-order scatter above and below the overall trend. Clearly, further experimental studies are needed between ΔFMQ +1 and +2 to quantify the relative roles of H_2O and fO_2 in driving calc-alkaline vs tholeiitic differentiation in arc magmas.

Other controls on THI

Our analysis above points to H_2O as the primary control on the early stages of magma differentiation that define the THI. Pressure and H_2O may be linked through vapor saturation, but pressure variations alone are unlikely to

cause the magnitude of THI variations observed. H_2O and fO_2 appear to co-vary at a global scale, but within the arc magma array most of the THI variation appears to be driven by H_2O variation within a limited range of elevated fO_2. Water suppresses plagioclase and enhances spinel crystallization, and these effects dominate the part of the liquid line of descent that governs magmatic differentiation from basalt to andesite. We have emphasized this early part of magmatic differentiation as it serves to link mafic magmas from multiple tectonic settings, and it records the greatest diversity of differentiation trends (i.e. most magmatic trends eventually reach Fe depletion and thus become CA at low MgO). However, there are several other processes that may be important as magmas continue to evolve to more silicic compositions, such as amphibole fractionation and crustal assimilation–magma mixing, or that affect primary magma compositions in a way that may also set the course of differentiation. We discuss these issues below, as they may modulate the water-driven variations, dominate certain magmatic systems, or take over as magmas evolve to more silicic compositions than reflected within the THI.

Amphibole fractionation

Although the focus is on less evolved magma compositions here, amphibole is commonly observed in arc andesites, dacites and rhyolites. Amphibole removes Fe from these silicic liquids (Kay & Kay, 1985), driving further Fe depletion and CA trends. Amphibole is not a ubiquitous phase, however, as it requires certain conditions to saturate: generally >3 wt % Na_2O, >3wt % H_2O in the melt and <1100°C magmatic temperatures (Cawthorn & O'Hara, 1976; Sisson & Grove, 1993*a*; Grove *et al.*, 2003). For example, the recent eruptive rocks of Anatahan volcano in the Marianas contain no amphibole, despite the silicic composition (58–61% SiO_2; Wade *et al.*, 2006). Either H_2O contents were too low (<3·4 wt % H_2O by difference; Pallister *et al.*, 2005), or temperatures were too high (980–1100°C two-pyroxene temperatures; deMoor *et al.*, 2005), to stabilize amphibole, so Fe depletion in these magmas must be driven by magnetite fractionation. Thus, there is a complex interplay of compositional parameters and degassing history that will dictate the influence of amphibole fractionation in generating Fe depletion and CA trends. In general, amphibole is much more common in magmas that are more evolved than those that contribute to the THI (i.e. <4% MgO).

The question of early amphibole fractionation also remains open. Davidson *et al.* (2007) argued for a pervasive amphibole effect on the rare earth element evolution of arc magmas (i.e. decreasing Dy/Yb with increasing SiO_2), even if amphibole is not observed in the volcanic products. They concluded that amphibole will help drive CA differentiation. Many of the magmas in the Davidson *et al.* study, however, develop strong Dy/Yb trends only after they have evolved beyond the compositional range of the THI, and other key suites (e.g. Anatahan, Seguam) show no amphibole effect at all. Nonetheless, the prevalence of this amphibole effect remains important to establish within the global arc dataset. Grove *et al.* (2003) presented experiments that demonstrate how high Mg-number amphibole (>77) may crystallize early in a magma sequence, but only at high pressures (>5 kbar) and very high H_2O contents (>10 wt %). Such amphiboles, however, generally have Fe contents too low (<10 wt %) to drive substantial Fe depletion in the early part of the LLD. Existing evidence thus points to the importance of amphibole fractionation on Fe depletion late in a magma's LLD, beyond the window of the THI, and generally after magnetite has already driven Fe depletion in wet, oxidized arc magmas.

Assimilation and magma mixing

Average upper continental crust and especially crustal melts have low FeO* and MgO contents that, when mixed with mafic magmas, will drive Fe depletion and CA trends. Coupled assimilation, crystallization and mixing have been documented in many magmatic systems and are major drivers of variation in magma compositions (e.g. Hildreth & Moorbath, 1988; Kay & Kay, 1994; Dungan & Davidson, 2004; Annen *et al.*, 2006). Although crustal assimilation may decrease THI, there is little evidence that it introduces H_2O into magmas. For example, partially to extensively melted granitoid blocks (probably the wall-rocks of the climactic magma chamber) discharged during final stages of the 7700 years BP eruption of Mt. Mazama were found to contain relatively anhydrous rhyolitic melt (Bacon *et al.*, 1989). In fact, in most examples considered here, melt inclusions with the highest H_2O contents are found in the most primitive olivines and basaltic compositions and decrease as the magma evolves (Electronic Appendix E; Luhr, 2001; Wade *et al.*, 2006; Benjamin *et al.*, 2007; Cooper, 2009; Roberge *et al.*, 2009). Although assimilation is a potentially important process in varying a magma's THI, there is little evidence that it can generate the global THI–H_2O array (Fig. 7b). Assimilation and magma mixing may lead to important second-order effects on THI, and we point to some examples below.

One classic example included here is Parícutin volcano, Mexico, which notably shifted composition roughly halfway through its 9 year eruption in a manner consistent with crustal assimilation (McBirney *et al.*, 1987). This shift occurs between 4 and 5 wt % MgO, and could affect the THI, although here we used MIs from samples that erupted prior to the shift in 1947 (Luhr, 2001). The MIs include compositions more primitive than any erupted, and contain up to 4 wt % H_2O in the earliest and most mafic erupted products (Luhr, 2001; Pioli *et al.*, 2008). These water contents, coupled with the lack of plagioclase

phenocrysts in the scoria, are consistent with Parícutin's calc-alkaline THI (0·81). Nevertheless, Parícutin scoria lacks magnetite or amphibole, so its low THI may reflect some amount of assimilation. Further melt inclusion studies might better resolve the crystallization path of this magma prior to the development of the strong assimilation path.

More recently, Hora *et al.* (2009) have proposed a direct connection between calc-alkaline differentiation trends (in the classic Miyashiro sense) and assimilation and mixing with silicic magmas in the upper crust, based on their detailed studies of Parinacota volcano, Chile. The magmatic evolution with time, coupled with changes in Th isotopic composition, led them to propose a mechanism that elaborates on earlier ideas that Myers *et al.* (1985) developed for Aleutian volcanoes, of 'clean' magmatic systems (e.g. rapid magma transport through the crust and TH trends) vs 'dirty' magmatic systems (e.g. stalling and assimilation in the upper crust and CA differentiation). Such a concept has figured strongly in the study of Aleutian magmas, where CA magmas generally record more evidence for assimilation and mixing (Kay & Kay, 1994; George *et al.*, 2003, 2004). However, virtually all of these observations have been made in volcanic rocks with <4 wt % MgO, outside the range of the THI (e.g. all of CA Parinacota, Hora *et al.*, 2009; all of CA Aniakchak, George *et al.*, 2004; Redoubt, George *et al.*, 2003; and Adak lavas showing $^{87}Sr/^{86}Sr$ variation, Myers *et al.*, 1985). All other factors being equal, crustal interactions will probably be greater for more silicic magmas, as they reflect a longer cooling history in the crust, and because assimilation can consume heat and thereby drive crystallization. Thus, although crustal assimilation is strongly implicated in silicic magmas, the extent to which mafic magmas are affected, and specifically those that contribute to the THI (>4% MgO), is less clear and warrants further study.

Another important process inferred in magma evolution is the mixing of cognate magmas. Mixing between mafic magmas and low-Fe felsic magmas, which have themselves experienced crustal assimilation or magnetite fractionation, will generate CA trends. Such mixing processes are commonly inferred from the presence of multiple populations of crystals or linear trends on variation diagrams. One relevant example is Augustine, where Roman *et al.* (2006) found evidence for magma mixing based on disequilibrium mineral textures and linear trends on Harker diagrams for recent andesite–dacite eruptive rocks. These trends, however, are generally not collinear with the more mafic volcanic products examined here, particularly for Al_2O_3 and TiO_2 (Zimmer, 2009). Most of the MgO–FeO* data for the Aleutians in Fig. 6 show kinks in the evolutionary paths (especially that for Shishaldin), more consistent with the appearance of new mineral phases along the liquid line of descent than with magma mixing. Thus the outstanding problem is whether the rich crystal cargo carried in some magmas is evidence for widespread mixing that affects the dominant liquid line of descent (Dungan & Davidson, 2004) or entrainment of xenocrysts that have a small compositional effect on the bulk-rock.

Assimilation and mixing with silicic magmas is a very important process governing the later parts of magma differentiation. The extent to which it drives TH and CA trends in the initial part of the LLD is less certain. Most of the observations made here in the development of the THI dataset are consistent with a predominant process of crystal fractionation and the control of H_2O on mineral assemblages. Further work involving melt inclusions, which in some cases include more mafic liquids not sampled in whole-rock populations (as in Parícutin; Luhr, 2001), and crystal populations, which may simultaneously record the magma's LLD and P–T path (Putirka, 2008), volatile content (Wade *et al.*, 2008), and isotopic composition (Ramos & Tepley, 2008), is a rich new line of inquiry that may help to distinguish crystal fractionation from assimilation and mixing over different parts of a magma's evolutionary path.

Bulk composition

Variations in primary magma composition will also affect crystallization sequences and thus THI (Grove & Baker, 1984; Miller *et al.*, 1992). Such variations include initial FeO* contents, which will affect the saturation temperature of Fe–Ti oxides, and the CaO/Al_2O_3 ratio, which will affect the clinopyroxene/plagioclase ratio. We explored these effects by varying FeO* and CaO/Al_2O_3 within the global range observed in arcs (6·5–12·5 wt % FeO* and 0·5–1·3 CaO/Al_2O_3; Plank & Langmuir, 1988) and assessed the impact on the THI using pMELTS. Results were in the expected direction, with increases in FeO* leading to crystallization of spinel at higher MgO, and a reduction of THI from 1·04 to 1·00, and increases in CaO/Al_2O_3 leading to earlier crystallization of higher Mg-number clinopyroxene, and a small increase in THI from 0·9 to 1·0. Thus, although variations in the major element composition of primary magmas will indeed affect the trend of magmatic evolution, we conclude they have a smaller effect on THI (5–10%) than that generated by varying H_2O (>40%).

One magma type that has not been discussed, but is relevant to the generation of CA magmas, is the adakite, or high Mg-number andesite, common to the western Aleutians (Kay, 1978; Yogodzinski *et al.*, 1994, 1995; Kelemen *et al.*, 2003). Although most arc magmas develop CA trends as they evolve to lower Mg-number, mantle–melt reaction may generate primary CA magmas (e.g. Kelemen, 1990). When melt from the eclogitized slab or mantle reacts with peridotite during ascent, a silica-oversaturated melt and a depleted mantle residue may form (Kelemen, 1990; Kelemen *et al.*, 1990; Baker *et al.*,

1994; Grove *et al.*, 2002), resulting in primary, high Mg-number andesites (Mg-number >0·6, 54–65 wt % SiO_2). Slab melting may occur where young, hot lithosphere is subducting (Defant & Drummond, 1990), and may be facilitated in the western Aleutians by a tear in the subducting slab (Yogodzinski *et al.*, 2001; Davaille & Lees, 2004; Lee *et al.*, 2009). In addition to the western Aleutian volcanoes, Shasta is the only volcano with a substantial number of high Mg-number andesites in Table 1, although two other volcanoes have fewer than 10% of the samples classified as high Mg-number andesites (Irazú and Stromboli). High Mg-number andesites are noted for their strong CA character on the FeO*/MgO–SiO_2 diagram as they are silicic yet have low FeO*/MgO (high Mg-number). These magmas are also CA by our definition, evolving with Fe depletion (THI <1). For example, Shasta has among the lowest THI (0·61) of any volcano; it is also among the wettest (>8% H_2O; Grove *et al.*, 2002). Other high Mg-number andesite suites are less extreme, with THI = 0·84 for Piip volcano in the western Aleutians (Yogodzinski *et al.*, 1994), and THI = 0·91 for the Setouchi volcanic belt of SW Japan (Tatsumi & Ishizaka, 1982; Shiraki *et al.*, 1991). No water measurements exist for these latter suites, so whether their CA evolution is a result of their unusual bulk composition or is largely a product of their water content (like other arc magmas) awaits new data.

THI: a predictive tool?

Measuring the water content in magmas is a meticulous process, generally restricted to the chance occurrence of large, glassy melt inclusions in early formed crystals. The additional requirement of rapidly cooled tephra further restricts melt inclusion studies to young samples (generally ≪1 Ma), as tephra weathers rapidly. Thus, many magmatic systems are inaccessible to volatile studies via melt inclusions, which thwarts efforts to understand the role of H_2O in driving melting, source heterogeneity, and eruption. Given the relationship in Fig. 7b, the THI may serve as a crude predictive tool for estimating magmatic water contents. The THI can be calculated for any magmatic suite that evolves from 8 to 4% MgO, and the 95% confidence interval on equation (2) gives H_2O with an average uncertainty of ± 1·2 wt %. Such uncertainties are comparable with that typical of sum deficit determinations (±1 wt % H_2O; Sisson & Layne, 1993; Devine *et al.*, 1995). Although this estimation will never be as precise as actual measurements, and the relationship can certainly be improved with additional data that allow more refined approaches, it is still useful in the context of arc magmas, where water content varies from ~2 to 7 wt % H_2O. The approach may be particularly useful for the study of ancient igneous rocks, where few other methods are available for estimating initial magmatic H_2O contents, especially if combined with estimates of fO_2.

Although caution must be exercised when using THI to predict magmatic water contents for any magmatic suite, this is particularly true for OIB magmas [which were excluded from the regression in Fig. 7b, and equation (2)]. The majority of LLDs for the magmas examined here reach maximum FeO* close to 4 wt % MgO, whereas OIB magmas attain maximum FeO* over a range from 3·9 to 6·2 wt % MgO, with the average at ~5 wt % MgO. For example, four Hawaiian volcanoes in Fig. 7b (Kilauea, Mauna Kea, Mauna Loa, and Loihi) have THI and maximum FeO* ranging from 0·92 to 1·16 and from 4·7 to 5·1 wt % MgO, respectively. If THI is calculated using $Fe_{8·0}$ and maximum FeO*, THI is much more uniform: 1·20–1·24. This range is more consistent with the measured water contents of 0·36–0·48 wt % (Hauri, 2002; Davis *et al.*, 2003; Seaman *et al.*, 2004). Mauna Loa exhibits slightly different behavior from the other volcanoes, with higher THI (1·38) that changes very little when maximum FeO* is used to calculate THI (1·42). The range of THI in OIB magmas in Fig. 4 is 0·76–1·20, and given the correlation between THI and H_2O in Fig. 7b, this suggests a large range in water contents in OIB magmas. However, reported water contents are rarely >2 wt % H_2O, often <1 wt %. This discrepancy indicates that other parameters may have a stronger effect than water on the timing of spinel crystallization and Fe depletion in OIB magmas. For example, most OIB magmas originate with very high Fe contents (generally >11 wt % $Fe_{8·0}$; Table 1), and this may lead to earlier spinel crystallization and a lower THI for a given water content. This illustrates the difficulty in finding one parameter to describe all magmas, and future work may elucidate a better predictive tool for OIB magmas.

The above also underscores the shortcomings of the THI. A better tool for quantifying Fe enrichment would take into account different points along the LLD where different magmas attain maximum Fe. However, such an approach would be difficult to apply to strongly calc-alkaline magmas, which display no Fe enrichment or maximum. In this way, the THI is easy to apply for magmas that enrich or deplete in Fe. A perfect dataset would define an LLD that would constrain the appearances, proportions, and compositions of phases along the cotectic. Knowledge of such crystallization sequences, either through perfect datasets, experimental studies of magma series, or fully accurate thermodynamic models, would clearly be beneficial in quantifying the calc-alkalinity of a magma and understanding its causes. In the lack of such perfect datasets and pervasive laboratory efforts, however, the THI is a simple tool that captures major differences in magmatic differentiation globally and within arcs. Future efforts to improve the THI may lead to a more precise tool for quantifying H_2O variations than is possible now.

CONCLUSIONS

In this study we have developed a new index of magma evolution, the Tholeiitic Index, $THI = Fe_{4\cdot0}/Fe_{8\cdot0}$. This index improves upon previous classification schemes by isolating the primary feature of tholeiitic evolution, Fe enrichment, without convoluting primary magma variations or evolution of silica or alkalis. The THI quantifies the continuum of Fe enrichment and depletion observed in magmatic suites globally and discriminates effectively between MOR, back-arc basin and arc magma evolution. The THI captures the early part of a liquid line of descent, where magmas diverge strongly in their Fe evolution, as opposed to the late stages, where most magmas converge in Fe depletion trends. Aleutian volcanoes span the range in THI, as well as water content in arc magmas, and conform to a global array where THI and H_2O strongly co-vary. The anti-correlation is consistent with a dominant control by H_2O on the early paths of magma differentiation. Water leads to calc-alkaline differentiation, as a result of the relative suppression of plagioclase and enhancement of spinel (magnetite) along the liquid line of descent from basalt to andesite. The magnitude of the effect is quantitatively consistent with the effects predicted from experimental studies and thermodynamic models, provided fO_2 varies in concert with H_2O globally (from ~FMQ to ΔFMQ +2). The THI may become a predictive tool for the H_2O contents of magmatic suites for which measurements are unavailable or impossible.

The potential control of H_2O on magma differentiation has long been predicted by petrologists and more recently determined by experimentalists, from the early proposal of Kennedy (1955) to the landmark experiments of Sisson & Grove (1993*a*, 1993*b*). The current study illustrates how these predictions are now observed in the growing database of measured magmatic water concentrations. These types of data have proliferated only in the past decade, and first-order studies are continuing for many volcanic arcs, such as for the Aleutians presented here. Direct measurements of H_2O in melt inclusions and glasses have taken the experimental predictions further, providing a quantitative relationship with the Tholeiitic Index that links magma evolution in different tectonic settings. A fundamental feature of modern terrestrial magmas is an apparent link between water content and oxidation state, which work together to create the extent of Fe depletion observed. Whether this relationship existed in the past and how much each parameter contributes to calc-alkaline differentiation remain areas for future work.

ACKNOWLEDGEMENTS

Samples for this study were generously donated by Fred Anderson (Emmons), Bob Kay (Akutan), and Jim Begét (Okmok). We are indebted to Mike Jackson of EarthScope/PBO for logistical support and sample collection, and to John Power and Chris Waythomas for helpful advice during Akutan fieldwork. Thanks go to the captain and crew of the R.V. *Tiglax*, the F.V. *Miss Alyssa* and the F.V. *Suzanne Marie* for safe passage and support of work on Seguam, Akutan and Unalaska. Field work was greatly assisted by Angie Roach, Kathryn Grover, and Kevin Hauri. Jianhua Wang, Neel Chatterjee, and Louise Bolge are thanked for patient assistance with analytical work. Statistical advice and assistance was kindly provided by Jeremy Zechar. We thank Madeline Humphreys, Adam Kent, and Ken Sims for very thorough and constructive reviews, and John Gamble for editorial handling of the manuscript.

FUNDING

This work was supported by the National Science Foundation (EAR-0409495 and EAR-0609953 to T.P. and E.H.H., and EAR-0233712 to T.P.) and Boston University (CAS Dean's Fellowship to M.M.Z.).

SUPPLEMENTARY DATA

Supplementary data for this paper are available at *Journal of Petrology* online.

REFERENCES

Albarède, F. (1992). How deep do common basaltic magmas form, differentiate? *Journal of Geophysical Research—Solid Earth* **97**, 10997–11009.

Anderson, A. T. J. (1979). Water in some hypersthenic magmas. *Journal of Geology* **87**, 509–531.

Annen, C., Blundy, J. D. & Sparks, R. S. J. (2006). The genesis of intermediate and silicic magmas in deep crustal hot zones. *Journal of Petrology* **47**, 505–539.

Arculus, R. J. (2003). Use and abuse of the terms calcalkaline and calcalkalic. *Journal of Petrology* **44**, 929–935.

Asimow, P. D. & Langmuir, C. H. (2003). The importance of water to oceanic mantle melting regimes. *Nature* **421**, 815–820.

Bacon, C. R., Adami, L. H. & Lanphere, M. A. (1989). Direct evidence for the origin of low-^{18}O silicic magmas: Quenched samples of a magma chamber's partially-fused granitoid walls. *Earth and Planetary Science Letters* **96**, 199–208.

Baker, D. R. & Eggler, D. H. (1987). Compositions of anhydrous and hydrous melts coexisting with plagioclase, augite, and olivine or low-Ca pyroxene from 1 atm to 8 kbar—Application to the Aleutian volcanic center of Atka. *American Mineralogist* **72**, 12–28.

Baker, M. B., Grove, T. L. & Price, R. (1994). Primitive basalts and andesites from the Mt Shasta region, N California—products of varying melt fraction and water-content. *Contributions to Mineralogy and Petrology* **118**, 111–129.

Baker, M. B., Hirschmann, M. M., Ghiorso, M. S. & Stolper, E. M. (1995). Compositions of near-solidus peridotite melts from experiments and thermodynamic calculations. *Nature* **375**, 308–311.

Benjamin, E. R., Plank, T., Wade, J. A., Kelley, K. A., Hauri, E. H. & Alvarado, G. E. (2007). High water contents in basaltic magmas from Irazú Volcano, Costa Rica. *Journal of Volcanology and Geothermal Research* **168**, 68–92.

Berndt, J., Koepke, J. & Holtz, F. (2005). An experimental investigation of the influence of water and oxygen fugacity on differentiation of MORB at 200 MPa. *Journal of Petrology* **46**, 135–167.

Bézos, A. & Humler, E. (2005). The $Fe^{3+}/\Sigma Fe$ ratios of MORB glasses and their implications for mantle melting. *Geochimica et Cosmochimica Acta* **69**, 711–725.

Blatter, D. L. & Carmichael, I. S. E. (1998). Hornblende peridotite xenoliths from central Mexico reveal the highly oxidized nature of subarc upper mantle. *Geology* **26**, 1035–1038.

Blundy, J. D. & Cashman, K. V. (2005). Rapid decompression-driven crystallization recorded by melt inclusions from Mount St. Helens volcano. *Geology* **33**, 793–796.

Bowen, N. L. (1928). *The Evolution of the Igneous Rocks*. Princeton, NJ: Princeton University Press.

Brandon, A. D. & Draper, D. S. (1996). Constraints on the origin of the oxidation state of mantle overlying subduction zones: An example from Simcoe, Washington, USA. *Geochimica et Cosmochimica Acta* **60**, 1739–1749.

Brophy, J. G. (1990). Andesites from northeastern Kanaga Island, Aleutians—Implications for calc-alkaline fractionation mechanisms and magma chamber development. *Contributions to Mineralogy and Petrology* **104**, 568–581.

Brophy, J. G., Whittington, C. S. & Park, Y. R. (1999). Sector-zoned augite megacrysts in Aleutian high alumina basalts: implications for the conditions of basalt crystallization and the generation of calc-alkaline series magmas. *Contributions to Mineralogy and Petrology* **135**, 277–290.

Canil, D., O'Neill, H. S. C., Pearson, D. G., Rudnick, R. L., McDonough, W. F. & Carswell, D. A. (1994). Ferric iron in peridotites and mantle oxidation states. *Earth and Planetary Science Letters* **123**, 205–220.

Carmichael, I. S. E. (1964). The petrology of Thingmuli, a Tertiary volcano in Eastern Iceland. *Journal of Petrology* **5**, 435–460.

Carmichael, I. S. E. (1991). The redox states of basic and silicic magmas—a reflection of their source regions. *Contributions to Mineralogy and Petrology* **106**, 129–141.

Carmichael, I. S. E. & Ghiorso, M. S. (1986). Oxidation–reduction relations in basic magma—a case for homogeneous equilibria. *Earth and Planetary Science Letters* **78**, 200–210.

Carr, M. J., Feigenson, M. D., Patino, L. C. & Walker, J. A. (2003). Volcanism and geochemistry in Central America: Progress and problems. In: Eiler, J. (ed.) *Inside the Subduction Factory, Geophysical Monograph, American Geophysical Union* **138**, 153–179.

Carroll, M. R. & Rutherford, M. J. (1988). Sulfur speciation in hydrous experimental glasses of varying oxidation-states—results from measured wavelength shifts of sulfur X-rays. *American Mineralogist* **73**, 845–849.

Cawthorn, R. G. & O'Hara, M. J. (1976). Amphibole fractionation in calc-alkaline magma genesis. *American Journal of Science* **276**, 309–329.

Chesner, C. A. & Rose, W. I. (1984). Geochemistry and evolution of the Fuego Volcanic Complex, Guatemala. *Journal of Volcanology and Geothermal Research* **21**, 25–44.

Christie, D. M., Carmichael, I. S. E. & Langmuir, C. H. (1986). Oxidation states of midocean ridge basalt glasses. *Earth and Planetary Science Letters* **79**, 397–411.

Cooper, L. B. (2009). Volatiles in Tonga Arc magmas and their role in unraveling subduction zone processes, PhD thesis, Boston University, Boston, MA, 411 pp.

Daley, E. E. (1986). Petrology, geochemistry, and the evolution of magmas from Augustine Volcano, Alaska, Master's thesis, University of Alaska, Fairbanks, AK, 103 pp.

Danyushevsky, L. V., Della-Pasqua, F. N. & Sokolov, S. (2000). Re-equilibration of melt inclusions trapped by magnesian olivine phenocrysts from subduction-related magmas: petrological implications. *Contributions to Mineralogy and Petrology* **138**, 68–83.

Danyushevsky, L. V., McNeill, A. W. & Sobolev, A. (2002). Experimental and petrological studies of melt inclusions in phenocrysts from mantle-derived magmas: an overview of techniques, advantages and complications. *Chemical Geology* **183**, 5–24.

Danyushevsky, L. V., Leslie, R. A. J., Crawford, A. J. & Durance, P. (2004). Melt inclusions in primitive olivine phenocrysts: The role of localized reaction processes in the origin of anomalous compositions. *Journal of Petrology* **45**, 2531–2553.

Davaille, A. & Lees, J. M. (2004). Thermal modeling of subducted plates: tear and hotspot at the Kamchatka corner. *Earth and Planetary Science Letters* **226**, 293–304.

Davidson, J., Turner, S., Handley, H., MacPherson, C. & Dosseto, A. (2007). Amphibole 'sponge' in arc crust? *Geology* **35**, 787–790.

Davis, M. G., Garcia, M. O. & Wallace, P. (2003). Volatiles in glasses from Mauna Loa volcano, Hawaii: Implications for magma degassing and contamination, and growth of Hawaiian volcanoes. *Contributions to Mineralogy and Petrology* **144**, 570–591.

Defant, M. J. & Drummond, M. S. (1990). Derivation of some modern arc magmas by melting of young subducted lithosphere. *Nature* **347**, 662–665.

deMoor, J. M., Fischer, T. P., Hilton, D. R., Hauri, E., Jaffe, L. A. & Camacho, J. T. (2005). Degassing at Anatahan volcano during the May 2003 eruption: implications from petrology, ash leachates, and SO_2 emissions. *Journal of Volcanology and Geothermal Research* **146**, 117–138.

Devine, J. D., Gardner, J. E., Brack, H. P., Layne, G. D. & Rutherford, M. J. (1995). Comparison of microanalytical methods for estimating H_2O contents of silicic volcanic glasses. *American Mineralogist* **80**, 319–328.

Dixon, J. E., Stolper, E. & Delaney, J. R. (1988). Infrared spectroscopic measurements of CO_2 and H_2O in Juan de Fuca Ridge basaltic glasses. *Earth and Planetary Science Letters* **90**, 87–104.

Dungan, M. A. & Davidson, J. (2004). Partial assimilative recycling of the mafic plutonic roots of arc volcanoes: An example from the Chilean Andes. *Geology* **32**, 773–776.

Eichelberger, J. C., Izbekov, P. E. & Browne, B. L. (2006). Bulk chemical trends at arc volcanoes are not liquid lines of descent. *Lithos* **87**, 135–154.

Falloon, T. J. & Danyushevsky, L. V. (2000). Melting of refractory mantle at 1·5, 2 and 2·5 GPa under anhydrous and H_2O-undersaturated conditions: Implications for the petrogenesis of high-Ca boninites and the influence of subduction components on mantle melting. *Journal of Petrology* **41**, 257–283.

Fenner, C. N. (1926). The Katmai magmatic province. *Journal of Geology* **34**, 673–772.

Fenner, C. N. (1931). The residual liquids of crystallizing magmas. *Mineralogical Magazine* **22**, 539–560.

Finney, B., Turner, S., Hawkesworth, C., Larsen, J., Nye, C., George, R., Bindeman, I. & Eichelberger, J. (2008). Magmatic differentiation at an island-arc caldera: Okmok Volcano, Aleutian Islands, Alaska. *Journal of Petrology* **49**, 857–884.

Ford, C. E., Russell, D. G., Craven, J. A. & Fisk, M. R. (1983). Olivine–liquid equilibria: temperature, pressure, and composition dependence of the crystal/liquid cation partition coefficients for Mg, Fe^{2+}, Ca, and Mn. *Journal of Petrology* **24**, 256–265.

Fournelle, J. H. (1988). Geology and petrology of Shishaldin volcano, Unimak Island, Aleutian Arc, Alaska, PhD thesis, Johns Hopkins University, Baltimore, MD, 507 pp.

Gaetani, G. A. & Grove, T. L. (1998). The influence of water on melting of mantle peridotite. *Contributions to Mineralogy and Petrology* **131**, 323–346.

Gaetani, G. A. & Watson, E. B. (2000). Open system behavior of olivine-hosted melt inclusions. *Earth and Planetary Science Letters* **183**, 27–41.

George, R., Turner, S., Hawkesworth, C., Morris, J., Nye, C., Ryan, J. & Zheng, S.-H. (2003). Melting processes and fluid and sediment transport rates along the Alaska–Aleutian arc from an integrated U–Th–Ra–Be isotope study. *Journal of Geophysical Research* **108**, doi:10.1029/2002JB001916.

George, R., Turner, S., Hawkesworth, C., Bacon, C. R., Nye, C., Stelling, P. & Dreher, S. (2004). Chemical versus temporal controls on the evolution of tholeiitic and calc-alkaline magmas at two volcanoes in the Alaska–Aleutian arc. *Journal of Petrology* **45**, 203–219.

Ghiorso, M. S. & Sack, R. O. (1995). Chemical mass transfer in magmatic processes. IV. A revised and internally consistent thermodynamic model for the interpolation and extrapolation of liquid–solid-equilibria in magmatic systems and elevated temperatures and pressures. *Contributions to Mineralogy and Petrology* **119**, 197–212.

Ghiorso, M. S., Hirschmann, M. M., Reiners, P. W. & Kress, V. C. (2002). The pMELTS: A revision of MELTS for improved calculation of phase relations and major element partitioning related to partial melting of the mantle to 3 GPa. *Geochemistry, Geophysics, Geosystems* **3**, doi:10.1029/2001GC000217.

Gill, J. B. (1981). *Orogenic Andesites and Plate Tectonics*. Berlin: Springer.

Grove, T. L. & Baker, M. B. (1984). Phase-equilibrium controls on the tholeiitic versus calc-alkaline differentiation trends. *Journal of Geophysical Research* **89**, 3253–3274.

Grove, T. L. & Bryan, W. B. (1983). Fractionation of pyroxene-phyric MORB at low pressure—An experimental study. *Contributions to Mineralogy and Petrology* **84**, 293–309.

Grove, T. L., Parman, S. W., Bowring, S. A., Price, R. & Baker, M. B. (2002). The role of a H_2O-rich fluid component in the generation of primitive basaltic andesites and andesites from the Mt. Shasta region, N. California. *Contributions to Mineralogy and Petrology* **142**, 375–396.

Grove, T. L., Elkins-Tanton, L. T., Parman, S. W., Chatterjee, N., Müntener, O. & Gaetani, G. A. (2003). Fractional crystallization and mantle-melting controls on calc-alkaline differentiation trends. *Contributions to Mineralogy and Petrology* **145**, 515–533.

Grove, T. L., Baker, M. B., Price, R. C., Parman, S. W., Elkins-Tanton, L. T., Chatterjee, N. & Müntener, O. (2005). Magnesian andesite and dacite lavas from Mt. Shasta, northern California: products of fractional crystallization of H2O-rich mantle melts. *Contributions to Mineralogy and Petrology* **148**, 542–565.

Gust, D. A. & Perfit, M. R. (1987). Phase-relations of a high-Mg basalt from the Aleutian island-arc—Implications for primary island-arc basalts and high-Al basalts. *Contributions to Mineralogy and Petrology* **97**, 7–18.

Harker, A. (1909). *The Natural History of Igneous Rocks*. London: Methuen.

Hauri, E. (2002). SIMS analysis of volatiles in silicate glasses, 2. Isotopes and abundances in Hawaiian melt inclusions. *Chemical Geology* **183**, 115–141.

Hauri, E., Wang, J. H., Dixon, J. E., King, P. L., Mandeville, C. & Newman, S. (2002). SIMS analysis of volatiles in silicate glasses 1. Calibration, matrix effects and comparisons with FTIR. *Chemical Geology* **183**, 99–114.

Hildreth, W. & Moorbath, S. (1988). Crustal contributions to arc magmatism in the Andes of Central Chile. *Contributions to Mineralogy and Petrology* **98**, 455–489.

Hirschmann, M. M., Baker, M. B. & Stolper, E. M. (1998). The effect of alkalis on the silica content of mantle-derived melts. *Geochimica et Cosmochimica Acta* **62**, 883–902.

Holmes, A. (1918). The basaltic rocks of the Arctic region. *Mineralogical Magazine* **18**, 180–223.

Hora, J. M., Singer, B. S., Wörner, G., Beard, B. L., Jicha, B. R. & Johnson, C. M. (2009). Shallow and deep crustal control on differentiation of calc-alkaline and tholeiitic magma. *Earth and Planetary Science Letters* **285**, 75–86.

Ibarrola Muñoz, E. (1970). Variability of basaltic magmas in the Eastern and Central Canary Islands. *Estudios Geologicos (Madrid)* **26**, 337–399.

Irvine, T. N. & Baragar, W. R. (1971). A guide to the chemical classification of the common igneous rocks. *Canadian Journal of Earth Sciences* **8**, 523–548.

Jicha, B. R. & Singer, B. S. (2006). Volcanic history and magmatic evolution of Seguam Island, Aleutian island arc, Alaska. *Geological Society of America Bulletin* **118**, 805–822.

Jicha, B. R., Singer, B. S., Beard, B. L. & Johnson, C. M. (2005). Contrasting timescales of crystallization and magma storage beneath the Aleutian Island arc. *Earth and Planetary Science Letters* **236**, 195–210.

Johnson, E. R., Wallace, P. J., Granados, H. D., Manea, V. C., Kent, A. J. R., Bindeman, I. N. & Donegan, C. S. (2009). Subduction-related volatile recycling and magma generation beneath Central Mexico: Insights from melt inclusions, oxygen isotopes and geodynamic models. *Journal of Petrology* **50**, 1729–1764.

Johnson, K. E., Harmon, R. S., Richardson, J. M., Moorbath, S. & Strong, D. F. (1996). Isotope and trace element geochemistry of Augustine Volcano, Alaska: Implications for magmatic evolution. *Journal of Petrology* **37**, 95–115.

Jugo, P. J., Luth, R. W. & Richards, J. P. (2005). Experimental data on the speciation of sulfur as a function of oxygen fugacity in basaltic melts. *Geochimica et Cosmochimica Acta* **69**, 497–503.

Juster, T. C., Grove, T. L. & Perfit, M. R. (1989). Experimental constraints on the generation of FeTi basalts, andesites, and rhyodacites at the Galapagos Spreading Center, 85°W and 95°W. *Journal of Geophysical Research—Solid Earth and Planets* **94**, 9251–9274.

Kavanagh, J. L., Menand, T. & Sparks, R. S. J. (2006). An experimental investigation of sill formation and propagation in layered elastic media. *Earth and Planetary Science Letters* **245**, 799–813.

Kay, R. W. (1978). Aleutian magnesian andesites: melts from subducted Pacific oceanic crust. *Journal of Volcanology and Geothermal Research* **4**, 117–132.

Kay, S. M. & Kay, R. W. (1985). Aleutian tholeiitic and calc-alkaline magma series. 1. The mafic phenocrysts. *Contributions to Mineralogy and Petrology* **90**, 276–290.

Kay, S. M. & Kay, R. W. (1994). Aleutian magmas in space and time. In: Plafker, G. & Berg, H. C. (eds) *The Geology of Alaska. The Geology of North America, Vol. G-1*. Boulder, CO: Geological Society of America, pp. 687–722.

Kay, S. M., Kay, R. W. & Citron, G. P. (1982). Tectonic controls on tholeiitic and calc-alkaline magmatism in the Aleutian Arc. *Journal of Geophysical Research* **87**, 4051–4072.

Kelemen, P. B. (1990). Reaction between ultramafic rock and fractionating basaltic magma. 1. Phase-relations, the origin of calc-alkaline magma series, and the formation of discordant dunite. *Journal of Petrology* **31**, 51–98.

Kelemen, P. B., Joyce, D. B., Webster, J. D. & Holloway, J. R. (1990). Reaction between ultramafic rock and fractionating basaltic

magma. 2. Experimental investigation of reaction between olivine tholeiite and harzburgite at 1150°C–1050°C and 5 Kb. *Journal of Petrology* **31**, 99–134.

Kelemen, P. B., Yogodzinski, G. M. & Scholl, D. W. (2003). Along-strike variations in the Aleutian Island Arc: Genesis of high Mg# andesite and implications for continental crust. In: Eiler, J. (ed.) *Inside the Subduction Factory. Geophysical Monograph, American Geophysical Union* **138**, 223–276.

Kelley, K. A. & Cottrell, E. (2009). Water and oxidation state of subduction zone magmas. *Science* **325**, 605–607.

Kelley, K. A., Plank, T., Ludden, J. & Staudigel, H. (2003). Composition of altered oceanic crust at ODP Sites 801 and 1149. *Geochemistry Geophysics Geosystems* **4**.

Kelley, K. A., Plank, T., Newman, S., Stolper, E. M., Grove, T. L., Parman, S. & Hauri, E. H. (2010). Mantle melting as a function of water content beneath the Mariana Arc. *Journal of Petrology* **51**, 1711–1738.

Kennedy, G. C. (1955). Some aspects of the role of water in rock melts. In: *The Crust of the Earth. Geological Society of America, Special Papers* **62**, 489–504.

Kersting, A. B. & Arculus, R. J. (1994). Klyuchevskoy Volcano, Kamchatka, Russia—The role of high-flux recharged, tapped, and fractionated magma chamber(s) in the genesis of high-Al_2O_3 from high-MgO basalt. *Journal of Petrology* **35**, 1–41.

Kinzler, R. J. & Grove, T. L. (1992). Primary magmas of midocean ridge basalts. 2. Applications. *Journal of Geophysical Research—Solid Earth* **97**, 6907–6926.

Kress, V. C. & Carmichael, I. S. E. (1991). The compressibility of silicate liquids containing Fe_2O_3 and the effect of composition, temperature, oxygen fugacity and pressure on their redox states. *Contributions to Mineralogy and Petrology* **108**, 82–92.

Krienitz, M. S., Haase, K. M., Mezger, K. & Shaikh-Mashail, M. A. (2007). Magma genesis and mantle dynamics at the Harrat Ash Shamah volcanic field (Southern Syria). *Journal of Petrology* **48**, 1513–1542.

Kuno, H. (1968). Differentiation of basalt magmas. In: Hess, H. H. & Poldervaart, A. A. (eds) *Basalts: the Poldervaart Treatise on Rocks of Basaltic Composition*. New York: Interscience, pp. 623–688.

Kushiro, I. (1972). Effect of water on the composition of magmas formed at high pressures. *Journal of Geophysical Research* **95**, 6885–6906.

Lange, R. A., Carmichael, I. S. E. & Renne, P. R. (1993). Potassic volcanism near Mono Basin, California—evidence for high water and oxygen fugacities inherited from subduction. *Geology* **21**, 949–952.

Langmuir, C. H. & Hanson, G. (1980). An evaluation of major element heterogeneity in the mantle sources of basalts. *Philosophical Transactions of the Royal Society of London, Series A* **297**, 383–407.

Langmuir, C. H., Klein, E. M. & Plank, T. (1992). Petrological systematics of mid-ocean ridge basalts: Constraints on melt generation beneath mid-ocean ridges. In: Phipps-Morgan, J., Blackman, D. K. & Sinton, J. (eds) *Mantle Flow and Melt Generation at Mid-Ocean Ridges. Geophysical Monograph, American Geophysical Union* **71**, 183–280.

Larsen, J. F., Neal, C., Schaefer, J., Beget, J. & Nye, C. (2007). Late Pleistocene and Holocene caldera-forming eruptions of Okmok Caldera, Aleutian Islands, Alaska. In: Eichelberger, J., Gordeev, E., Izbekov, P., Kasahara, M. & Lees, J. (eds) *Volcanism and Subduction: The Kamchatka Region. Geophysical Monograph, American Geophysical Union* **172**, 343–364.

Lee, C.-T. A., Leeman, W. P., Canil, D. & Li, Z. X. A. (2005). Similar V/Sc systematics in MORB and arc basalts: Implications for the oxygen fugacities of their mantle source regions. *Journal of Petrology* **46**, 2313–2336.

Lee, C.-T. A., Luffi, P., Plank, T., Dalton, H. & Leeman, W. P. (2009). Constraints on the depths and temperatures of basaltic magma generation on Earth and other terrestrial planets using new thermobarometers for mafic magmas. *Earth and Planetary Science Letters* **279**, 20–33.

Luhr, J. F. (2001). Glass inclusions and melt volatile contents at Parícutin Volcano, Mexico. *Contributions to Mineralogy and Petrology* **142**, 261–283.

Mackwell, S. J. & Kohlstedt, D. L. (1990). Diffusion of hydrogen in olivine: Implications for water in the mantle. *Journal of Geophysical Resesarch* **95**, 5079–5088.

Macpherson, C. G., Dreher, S. T. & Thirlwall, M. F. (2006). Adakites without slab melting: High pressure differentiation of island arc magma, Mindanao, the Philippines. *Earth and Planetary Science Letters* **243**, 581–593.

Mandeville, C. W., Webster, J. D., Tappen, C., Taylor, B. E., Timbal, A., Sasaki, A., Hauri, E. & Bacon, C. R. (2009). Stable isotope and petrologic evidence for open-system degassing during the climactic and pre-climactic eruptions of Mt. Mazama, Crater Lake, Oregon. *Geochimica et Cosmochimica Acta* **73**, 2978–3012.

Martin, H., Smithies, R. H., Rapp, R., Moyen, J. F. & Champion, D. (2005). An overview of adakite, tonalite–trondhjemite–granodiorite (TTG), and sanukitoid: relationships and some implications for crustal evolution. *Lithos* **79**, 1–24.

Mathez, E. A. (1984). Influence of degassing on oxidation-states of basaltic magmas. *Nature* **310**, 371–375.

McBirney, A. R., Taylor, H. P. & Armstrong, R. L. (1987). Parícutin reexamined—a classic example of crustal assimilation in calc-alkaline magma. *Contributions to Mineralogy and Petrology* **95**, 4–20.

McConnell, V. S., Beget, J. E., Roach, A. L., Bean, K. W. & Nye, C. J. (1998). *Geologic map of the Makushin volcanic field, Unalaska Island, Alaska. Alaska Division of Geological & Geophysical Surveys Report of Investigations*, unpaged, 2 sheets.

Meijer, A. & Reagan, M. (1981). Petrology and geochemistry of the Island of Sarigan in the Mariana arc; Calc-alkaline volcanism in an oceanic setting. *Contributions to Mineralogy and Petrology* **77**, 337–354.

Métrich, N. & Clocchiatti, R. (1996). Sulphur abundance and its speciation in oxidized alkaline melts. *Geochimica et Cosmochimica Acta* **60**, 4151–4160.

Métrich, N., Bonnin-Mosbah, M., Menez, B. & Galoisy, L. (2002). Presence of sulfite (S^{IV}) in arc magmas: implications for volcanic sulfur emissions. *Geophysical Research Letters* **29**, doi:10.1029/2001GL014607.

Métrich, N., Berry, A. J., O'Neill, H. S. C. & Susini, J. (2009). The oxidation state of sulfur in synthetic and natural glasses determined by X-ray absorption spectroscopy. *Geochimica et Cosmochimica Acta* **73**, 2382–2399.

Michael, P. J. (1988). The concentration, behaviour and storage of H_2O in the suboceanic upper mantle: implications for mantle metasomatism. *Geochimica et Cosmochimica Acta* **52**, 555–566.

Miller, D. M., Langmuir, C. H., Goldstein, S. L. & Franks, A. L. (1992). The importance of parental magma composition to calc-alkaline and tholeiitic evolution—Evidence from Umnak Island in the Aleutians. *Journal of Geophysical Research—Solid Earth* **97**, 321–343.

Miyashiro, A. (1974). Volcanic rock series in island arcs and active continental margins. *American Journal of Science* **274**, 321–355.

Moore, G. & Carmichael, I. S. E. (1998). The hydrous phase equilibra (to 3 kbar) of an andesite and basaltic andesite from western

Mexico: Constraints on water content and conditions of phenocryst growth. *Contributions to Mineralogy and Petrology* **130**, 304–309.

Muñoz García, M. (1969). Petrology and the alkaline formations of Fuerteventura, Canary Islands. *Estudios Geologicos (Madrid)* **25**, 257–310.

Müntener, O., Kelemen, P. B. & Grove, T. L. (2001). The role of H_2O during crystallization of primitive arc magmas under uppermost mantle conditions and genesis of igneous pyroxenites: an experimental study. *Contributions to Mineralogy and Petrology* **141**, 643–658.

Myers, J. D., Marsh, B. D. & Sinha, A. K. (1985). Strontium isotopic and selected trace-element variations between two Aleutian volcanic centers (Adak and Atka)—Implications for the development of arc volcanic plumbing systems. *Contributions to Mineralogy and Petrology* **91**, 221–234.

Newman, S. & Lowenstern, J. B. (2002). VOLATILECALC: A silicate–melt–H_2O–CO_2 solution model written in Visual Basic for Excel. *Computers and Geosciences* **28**, 597–604.

Nilsson Farley, K. (1994). Oxidation state and sulfur concentrations in Lau Basin basalts. In: Hawkins, J., Parson, L. & Allan, J. *et al.* (eds) *Proceedings of the Ocean Drilling Program, Scientific Results, 135.* College Station, TX: Ocean Drilling Program, pp. 603–613.

Nye, C. & Reid, M. (1986). Geochemistry of primary and least-fractionated lavas from Okmok volcano, central Aleutians: Implications for arc magma genesis. *Journal of Geophysical Research* **91**, 10271–10287.

Osborn, E. F. (1959). Role of oxygen pressure in the crystallization and differentiation of basaltic magma. *American Journal of Science* **257**, 609–647.

Pallister, J. S., Trusdell, F. A., Brownfield, I. K., Siems, D. F. & Camacho, J. T. (2005). Phreatomagmatic eruptions of Anatahan volcano: Stratigraphy and petrology of the erupted products. *Journal of Volcanology and Geothermal Research* **146**, 208–225.

Parkinson, I. J. & Arculus, R. J. (1999). The redox state of subduction zones: insights from arc-peridotites. *Chemical Geology* **160**, 409–423.

Parman, S. W. & Grove, T. L. (2004). Harzburgite melting with and without H2O: Experimental data and predictive modeling. *Journal of Geophysical Research—Solid Earth* **109**, doi:10.1029/2003JB002566.

Patrick, M. R., Dehn, J., Papp, K. R., Lu, Z., Dean, K., Moxey, L., Izbekov, P. & Guritz, R. (2003). The 1997 eruption of Okmok Volcano, Alaska: a synthesis of remotely sensed imagery. *Journal of Volcanology and Geothermal Research* **127**, 87–105.

Peacock, M. A. (1931). Classification of igneous rock series. *Journal of Geology* **39**, 54–67.

Pioli, L., Erlund, E., Johnson, E., Cashman, K., Wallace, P., Rosi, M. & Delgado Granados, H. (2008). Explosive dynamics of violent Strombolian eruptions: the eruption of Parícutin Volcano 1943–1952 (Mexico). *Earth and Planetary Science Letters* **271**, 359–368.

Plank, T. & Langmuir, C. H. (1988). An evaluation of the global variations in the major element chemistry of arc basalts. *Earth and Planetary Science Letters* **90**, 349–370.

Plank, T. & Langmuir, C. H. (1998). The chemical composition of subducting sediment and its consequences for the crust and mantle. *Chemical Geology* **145**, 325–394.

Portnyagin, M., Almeev, R., Matveev, S. & Holtz, F. (2008). Experimental evidence for rapid water exchange between melt inclusions in olivine and host magma. *Earth and Planetary Science Letters* **272**, 541–552.

Putirka, K. (2008). Excess temperatures at ocean islands: Implications for mantle layering and convection. *Geology* **36**, 283–286.

Ramos, F. C. & Tepley, F. J. I. (2008). Inter- and intracrystalline isotopic disequilibria: techniques and applications. In: Putirka, K. D. & Tepley, F. J., III (eds) *Minerals, Inclusions and Volcanic Processes. Mineralogical Society of America and Geochemical Society, Reviews in Mineralogy and Geochemistry* **69**, 403–443.

Rapp, R. P. & Watson, E. B. (1995). Dehydration melting of metabasalt at 8–32 kbar: Implications for continental growth and crust–mantle recycling. *Journal of Petrology* **36**, 891–931.

Richter, D. H., Waythomas, C. F., McGimsey, R. G. & Stelling, P. L. (1998). *Geologic map of Akutan Island, Alaska. Geological Survey Open-File Report* **22.**

Roberge, J., Delgado-Granados, H. & Wallace, P. J. (2009). Mafic magma recharge supplies high CO_2 and SO_2 gas fluxes from Popocatepetl volcano, Mexico. *Geology* **37**, 107–110.

Roedder, P. L. & Emslie, R. F. (1970). Olivine–liquid equilibrium. *Contributions to Mineralogy and Petrology* **29**, 275–289.

Rogers, N. W., Hawkesworth, C. J. & Ormerod, D. S. (1995). Late Cenozoic basaltic magmatism in the western Great Basin, California and Nevada. *Journal of Geophysical Research—Solid Earth* **100**, 10287–10301.

Roman, D. C., Cashman, K. V., Gardner, C. A., Wallace, P. J. & Donovan, J. J. (2006). Storage and interaction of compositionally heterogeneous magmas from the 1986 eruption of Augustine Volcano, Alaska. *Bulletin of Volcanology* **68**, 240–254.

Rowe, M. C., Nielsen, R. L. & Kent, A. J. R. (2006). Anomalously high Fe contents in rehomogenized olivine-hosted melt inclusions from oxidized magmas. *American Mineralogist* **91**, 82–91.

Rowe, M. C., Kent, A. J. R. & Nielsen, R. L. (2009). Subduction influence on oxygen fugacity and trace and volatile elements in basalts across the Cascade Volcanic Arc. *Journal of Petrology* **50**, 61–91.

Schiano, P., Eiler, J. M., Hutcheon, I. D. & Stolper, E. M. (2000). Primitive CaO-rich, silica-undersaturated melts in island arcs: evidence for the involvement of clinopyroxene-rich lithologies in the petrogenesis of arc magmas. *Geochemistry, Geophysics, Geosystems* **1.**

Seaman, C., Sherman, S. B., Garcia, M. O., Baker, M. B., Balta, B. & Stolper, E. (2004). Volatiles in glasses from the HSDP2 drill core. *Geochemistry, Geophysics, Geosystems* **5**, doi:10.1029/2003GC000596.

Shiraki, K., Nagao, K., Takashi, N., Kakubuchi, S. & Matsumoto, Y. (1991). Trace element characteristics of the Setouchi volcanic rocks from Western Setonaikai. *Journal of the Japanese Association of Mineralogy, Petrology, and Economic Geology* **86**, 459–472.

Singer, B. S., Myers, J. D. & Frost, C. D. (1992). Mid-Pleistocene basalt from the Seguam volcanic center, central Aleutian Arc, Alaska: local lithospheric structures and source variability in the Aleutian Arc. *Journal of Geophysical Research* **97**, 4561–4578.

Sisson, T. W. & Bacon, C. R. (1999). Gas-driven filter pressing in magmas. *Geology* **27**, 613–616.

Sisson, T. W. & Grove, T. L. (1993*a*). Experimental investigations of the role of H_2O in calc-alkaline differentiation and subduction zone magmatism. *Contributions to Mineralogy and Petrology* **113**, 143–166.

Sisson, T. W. & Grove, T. L. (1993*b*). Temperatures and H_2O contents of low-MgO high-alumina basalts. *Contributions to Mineralogy and Petrology* **113**, 167–184.

Sisson, T. W. & Layne, G. D. (1993). H_2O in basalt and basaltic andesite glass inclusions from 4 subduction-related volcanoes. *Earth and Planetary Science Letters* **117**, 619–635.

Sparks, R. S. J. (1988). Petrology and geochemistry of the Loch Ba Ring-Dyke, Mull (NW Scotland)—An example of the extreme differentiation of tholeiitic magmas. *Contributions to Mineralogy and Petrology* **100**, 446–461.

Stelling, P., Beget, J., Nye, C., Gardner, J., Devine, J. D. & George, R. M. M. (2002). Geology and petrology of ejecta from the 1999 eruption of Shishaldin Volcano, Alaska. *Bulletin of Volcanology* **64**, 548–561.

Sutton, S. R., Karner, J. M., Papike, J. J., Delaney, J. S., Shearer, C. K., Newville, M., Eng, P., Rivers, M. & Dyar, M. D. (2005). Vanadium K edge XANES of synthetic and natural basaltic glasses and application to microscale oxygen barometry. *Geochimica et Cosmochimica Acta* **69**, 2333–2348.

Syracuse, E. M. & Abers, G. A. (2006). Global compilation of variations in slab depth beneath arc volcanoes and implications. *Geochemistry, Geophysics, Geosystems* **7**, doi:10.1029/2005GC001045.

Tappen, C. M., Webster, J. D., Mandeville, C. W. & Roderick, D. (2009). Petrology and geochemistry of ca. 2100–1000 a.B.P. magmas of Augustine volcano, Alaska, based on analysis of prehistoric pumiceous tephra. *Journal of Volcanology and Geothermal Research* **183**, 42–62.

Tatsumi, Y. (1981). Melting experiments on a high-magnesian andesite. *Earth and Planetary Science Letters* **54**, 357–365.

Tatsumi, Y. & Ishizaka, K. (1981). Existence of andesitic primary magma: an example from southwest Japan. *Earth and Planetary Science Letters* **53**, 124–130.

Tatsumi, Y. & Ishizaka, K. (1982). Origin of high-magnesium andesites in the Setouchi volcanic belt, southwest Japan, I. Petrological and chemical characteristics. *Earth and Planetary Science Letters* **60**, 293–304.

Thirlwall, M. F., Singer, B. S. & Marriner, G. F. (2000). ^{39}Ar–^{40}Ar ages and geochemistry of the basaltic shield stage of Tenerife, Canary Islands, Spain. *Journal of Volcanology and Geothermal Research* **103**, 247–297.

Trua, T., Deniel, C. & Mazzuoli, R. (1999). Crustal control in the genesis of Plio-Quaternary bimodal magmatism of the Main Ethiopian Rift (MER): geochemical and isotopic (Sr, Nd, Pb) evidence. *Chemical Geology* **155**, 201–231.

Vergniolle, S. & Caplan-Auerbach, J. (2006). Basaltic thermals and subplinian plumes: Constraints from acoustic measurements at Shishaldin volcano, Alaska. *Bulletin of Volcanology* **68**, 611–630.

Villiger, S., Ulmer, P., Muntener, O. & Thompson, A. B. (2004). The liquid line of descent of anhydrous, mantle-derived, tholeiitic liquids by fractional and equilibrium crystallization—an experimental study at 1·0 GPa. *Journal of Petrology* **45**, 2369–2388.

Vogel, T. A., Patino, L. C., Eaton, J. K., Valley, J. W., Rose, W. I., Alvarado, G. E. & Viray, E. L. (2006). Origin of silicic magmas along the Central American volcanic front: Genetic relationship to mafic melts. *Journal of Volcanology and Geothermal Research* **156**, 217–228.

Wade, J. A., Plank, T., Melson, W. G., Soto, G. J. & Hauri, E. H. (2006). The volatile content of magmas from Arenal volcano, Costa Rica. *Journal of Volcanology and Geothermal Research* **157**, 94–120.

Wade, J. A., Plank, T., Zimmer, M. M., Hauri, E., Roggensack, K. & Kelley, K. (2008). Prediction of magmatic water contents via measurement of H_2O in clinopyroxene phenocrysts. *Geology* **36**, 799–802.

Wager, L. R. & Deer, W. A. (1939). Geological investigations in East Greenland, III: The petrology of the Skaergaard Intrusion, Kangerdlugssuaq, East Greenland. *Meddelelser om Grønland* **105**, 1–352.

Walker, D., Shibata, T. & DeLong, S. E. (1979). Abyssal tholeiites from the Oceanographer Fracture Zone. II. Phase equilibria and mixing. *Contributions to Mineralogy and Petrology* **70**, 111–125.

Walker, J. A. & Carr, M. J. (1986). Compositional variations caused by phenocryst sorting at Cerro Negro volcano, Nicaragua. *Geological Society of America Bulletin* **97**, 1156–1162.

Wallace, P. & Carmichael, I. S. E. (1992). Sulfur in basaltic magmas. *Geochimica et Cosmochimica Acta* **56**, 1863–1874.

Wallace, P. J. (2005). Volatiles in subduction zone magmas: concentrations and fluxes based on melt inclusion and volcanic gas data. *Journal of Volcanology and Geothermal Research* **140**, 217–240.

Wallace, P. J. & Carmichael, I. S. E. (1994). S-speciation in submarine basaltic glasses as determined by measurements of SK-alpha X-ray wavelength shifts. *American Mineralogist* **79**, 161–167.

Wang, K., Plank, T., Walker, J. D. & Smith, E. I. (2002). A mantle melting profile across the Basin and Range, SW USA. *Journal of Geophysical Research—Solid Earth* **107**, doi:10.1029/2001JB000209.

Waythomas, C. F. (1999). Stratigraphic framework of Holocene volcaniclastic deposits, Akutan Volcano, east–central Aleutian Islands, Alaska. *Bulletin of Volcanology* **61**, 141–161.

Wiebe, R. A. (1997). Fe-rich tholeiitic liquids and their cumulate products in the Pleasant Bay layered intrusion, coastal Maine. *Contributions to Mineralogy and Petrology* **129**, 255–267.

Yoder, H. S. (1954). The system diopside–anorthite–water. *Annual Report to the Director of the Geophysical Laboratory for 1953–1954* 106–107.

Yogodzinski, G. M., Volynets, O. N., Koloskov, A. V., Seliverstov, N. I. & Matvenkov, V. V. (1994). Magnesian andesites and the subduction component in a strongly calc-alkaline series at Piip volcano, far western Aleutians. *Journal of Petrology* **35**, 163–204.

Yogodzinski, G. M., Kay, R. W., Volynets, O. N., Koloskov, A. V. & Kay, S. M. (1995). Magnesian andesite in the western Aleutian Komandorsky region—Implications for slab melting and processes in the mantle wedge. *Geological Society of America Bulletin* **107**, 505–519.

Yogodzinski, G. M., Lees, J. M., Churikova, T. G., Dorendorf, F., Woerner, G. & Volynets, O. N. (2001). Geochemical evidence for the melting of subducting oceanic lithosphere at plate edges. *Nature* **409**, 500–504.

Young, D. A. (1998). *N. L. Bowen and Crystallization–Differentiation: The Evolution of a Theory*. Washington, DC: Mineralogical Society of America.

Zimmer, M. M. (2009). Water in Aleutian magmas: Its origin in the subduction zone and its effects on magma evolution, PhD thesis, Boston University, Boston, MA, 448 pp.